NAVAL POSTGRADUATE SCHOOL

MONTEREY, CALIFORNIA

THESIS

TERRAIN AIDED NAVIGATION FOR REMUS AUTONOMOUS UNDERWATER VEHICLE

by

Jacob T. Juriga

June 2014

Thesis Advisor: Doug Horner
Second Reader: Noel DuToit

Approved for public release; distribution is unlimited

THIS PAGE INTENTIONALLY LEFT BLANK

REPORT DOCUMENTATION PAGE		*Form Approved OMB No. 0704-0188*

Public reporting burden for this collection of information is estimated to average 1 hour per response, including the time for reviewing instruction, searching existing data sources, gathering and maintaining the data needed, and completing and reviewing the collection of information. Send comments regarding this burden estimate or any other aspect of this collection of information, including suggestions for reducing this burden, to Washington headquarters Services, Directorate for Information Operations and Reports, 1215 Jefferson Davis Highway, Suite 1204, Arlington, VA 22202-4302, and to the Office of Management and Budget, Paperwork Reduction Project (0704-0188) Washington DC 20503.

1. AGENCY USE ONLY *(Leave blank)*	2. REPORT DATE June 2014	3. REPORT TYPE AND DATES COVERED Master's Thesis	
4. TITLE AND SUBTITLE TERRAIN AIDED NAVIGATION FOR REMUS AUTONOMOUS UNDERWATER VEHICLE		**5. FUNDING NUMBERS**	
6. AUTHOR(S) Jacob T. Juriga			
7. PERFORMING ORGANIZATION NAME(S) AND ADDRESS(ES) Naval Postgraduate School Monterey, CA 93943-5000		**8. PERFORMING ORGANIZATION REPORT NUMBER**	
9. SPONSORING /MONITORING AGENCY NAME(S) AND ADDRESS(ES) N/A		**10. SPONSORING/MONITORING AGENCY REPORT NUMBER**	
11. SUPPLEMENTARY NOTES The views expressed in this thesis are those of the author and do not reflect the official policy or position of the Department of Defense or the U.S. Government. IRB protocol number ____N/A____.			
12a. DISTRIBUTION / AVAILABILITY STATEMENT Approved for public release; distribution is unlimited		**12b. DISTRIBUTION CODE** A	

13. ABSTRACT (maximum 200 words)

This research investigates the ability to create an undersea bathymetry map and navigate relative to the map. This is known as terrain aided navigation (TAN). In our particular case, the goal was for an autonomous underwater vehicle (AUV) to reduce positional uncertainty through the use of downward-looking swath sonar and employing TAN techniques. This is considered important for undersea operations where positioning systems such as GPS are either not available or difficult to put in place. There are several challenges associated with TAN that are presented: The image processing necessary to extract altitude data from the sonar image, the initial building of the bathymetry map, incorporating a system and measurement model that takes into consideration AUV motion and sensor uncertainty and near-optimal, real-time estimation algorithms. The thesis presents a methodology coupled with analysis on datasets collected from joint Naval Postgraduate School/National Aeronautical Space Administration experimentation conducted at the Aquarius undersea habitat near Key Largo, Florida.

.

14. SUBJECT TERMS Terrain aided navigation, terrain-relative navigation, terrain-based navigation, autonomous underwater vehicle, particle filter, Kalman filter		**15. NUMBER OF PAGES** 77	
		16. PRICE CODE	
17. SECURITY CLASSIFICATION OF REPORT Unclassified	**18. SECURITY CLASSIFICATION OF THIS PAGE** Unclassified	**19. SECURITY CLASSIFICATION OF ABSTRACT** Unclassified	**20. LIMITATION OF ABSTRACT** UU

THIS PAGE INTENTIONALLY LEFT BLANK

TERRAIN AIDED NAVIGATION FOR REMUS AUTONOMOUS UNDERWATER VEHICLE

Jacob T. Juriga
Ensign, United States Navy
B.S., United States Naval Academy, 2013

Submitted in partial fulfillment of the
requirements for the degree of

MASTER OF SCIENCE IN MECHANICAL ENGINEERING

from the

NAVAL POSTGRADUATE SCHOOL
June 2014

Author: Jacob T. Juriga

Approved by: Doug Horner
                   Thesis Advisor

                   Noel Du Toit
                   Second Reader

                   Garth Hobson
                   Chair, Department of Mechanical Engineering

THIS PAGE INTENTIONALLY LEFT BLANK

ABSTRACT

This research investigates the ability to create an undersea bathymetry map and navigate relative to the map. This is known as terrain aided navigation (TAN). In our particular case, the goal was for an autonomous underwater vehicle (AUV) to reduce positional uncertainty through the use of downward-looking swath sonar and employing TAN techniques. This is considered important for undersea operations where positioning systems such as GPS are either not available or difficult to put in place. There are several challenges associated with TAN that are presented: The image processing necessary to extract altitude data from the sonar image, the initial building of the bathymetry map, incorporating a system and measurement model that takes into consideration AUV motion and sensor uncertainty and near-optimal, real-time estimation algorithms. The thesis presents a methodology coupled with analysis on datasets collected from joint Naval Postgraduate School/National Aeronautical Space Administration experimentation conducted at the Aquarius undersea habitat near Key Largo, Florida.

THIS PAGE INTENTIONALLY LEFT BLANK

TABLE OF CONTENTS

THIS PAGE INTENTIONALLY LEFT BLANK

LIST OF FIGURES

THIS PAGE INTENTIONALLY LEFT BLANK

LIST OF TABLES

THIS PAGE INTENTIONALLY LEFT BLANK

LIST OF ACRONYMS AND ABBREVIATIONS

ADCP	acoustic Doppler current profiler
AUV	autonomous underwater vehicle
CAVR	Center for Autonomous Vehicle Research
CEPR	circular error probable rate
DVL	Doppler velocity log
EKF	extended Kalman filter
GPS	Global Positioning System
INS	inertial navigation system
JSC	Johnson Space Center
LBL	long baseline (navigation system)
MAD	mean absolute difference
MBARI	Monterey Bay Aquarium Research Institute
MSD	mean square distance
NASA	National Aeronautical Space Administration
NEEMO	NASA Extreme Environment Mission Operations
NPS	Naval Postgraduate School
NXCOR	normalized cross-correlation
PF	particle filter
PMF	point mass filter
REMUS	Remote Environmental Monitoring UnitS
SIR	sequential importance resampling
SIS	sequential importance sampling
SLAM	simultaneous localization and mapping
TAN	terrain aided navigation
USBL	ultra-short baseline (navigation system)
XCOR	cross correlation

THIS PAGE INTENTIONALLY LEFT BLANK

ACKNOWLEDGMENTS

THIS PAGE INTENTIONALLY LEFT BLANK

I.   INTRODUCTION

A.   MOTIVATION FOR THIS WORK

A fundamental requirement for unmanned systems is the ability to accurately estimate position. The ubiquitous Global Position System (GPS) is used for a wide variety of aerial, surface and ground vehicles, but it has limitations—the signal can be jammed or occluded. What is desired is a robust methodology for position estimation that is not dependent upon an external system of navigational beacons.

One alternative is terrain aided navigation (TAN). It is a technique that uses onboard, exteroceptive ranging sensors as a navigational aid. Seminal work developing TAN methods was first completed in the terrain contour matching (TERCOM) algorithm employed upon cruise missiles in the 1960s, before GPS was available. While the advent of GPS alleviated some of the motivation for further TAN work, it remained a viable option for undersea localization since GPS signals cannot significantly penetrate the water surface.

Currently, commercial AUV systems rely heavily upon a costly, high-grade inertial navigation system (INS) in order to estimate the state of the vehicle. However, due to the dead-reckoning nature of INS systems, they are susceptible to drift over time. Unless localized by some other means, the vehicle's positional uncertainty grows without bound. Typically, this growing uncertainty is corrected through the aid of either a network of acoustic ranging transponders or resurfacing for a GPS fix. Both methods are at the least an inconvenience, and at most are unrealistic, costly, and potentially mission threatening. TAN presents an appealing alternative method of localization for an underwater vessel that can be implemented real-time with sensors already onboard.

B.   ENABLING TECHNOLOGIES

While TERCOM was first implemented in cruise missiles in the 1960s, the lack of necessary sensor accuracy, computational power, and data storage, along with other challenges associated with the undersea environment, have greatly delayed TAN implementation in the undersea domain [1]. For the last 35 years, the world has seen

remarkable improvements in computational power and data storage, as well as sensor accuracy. The increased processing power and data storage capabilities have not only significantly enhanced the accuracy of past, proven methods of TAN, but have also enabled the implementation of newer, more computationally expensive algorithms. A comparison of different methods for TAN is covered in Section D as well as in Chapter IV.

C.   PROBLEM DESCRIPTION

TAN, unlike the related field of simultaneous localization and mapping (SLAM), requires a prior map of the region. The overarching goal of TAN is to effectively use the prior terrain map in conjunction with new sensor information in order to aid in the navigation of the vehicle. Therefore, the work presented in this thesis can be separated into two main subject areas: Building an accurate bathymetry map and using the built map as a navigational aid.

First, a feature rich bathymetric map must be built. The map building process requires sonar image processing, a coordinate transformation between the vehicle's body-fixed reference frame and a global frame, and a possible interpolation of the data points in the global frame. There are many challenges and considerations that must be made within the scope of building an accurate bathymetry map. One of the more significant concerns affecting map accuracy is the growing positional uncertainty of the vehicle as a function of distance. Other considerations include specific image processing techniques and threshold selections. For example, including the sonar response from a large fish in the map would not be a useful feature for subsequent localization. Ensuring abrupt changes in bottom topography are incorporated to the bathymetry map would be very important.

The second main component of this work is implementing a method of TAN. TAN requires an algorithm that can effectively and accurately localize the position of the underwater vehicle based upon the previously built bathymetric map. There are several methods that can be used to varying degrees of success to accomplish this task. First, a kinematics motion model must be determined for the AUV. It is worth noting that the

kinematics for AUVs can be nonlinear, though they are often approximately well by a linearization [2]. Similarly, a measurement model must be formulated that encapsulates both the measurements and measurement noise. The exteroceptive measurements of the terrain are often highly non-linear as a result of the multiple peaks and valleys associated with the terrain. After appropriately modeling the vehicle and measurements, the TAN problem requires a correlation, or similarity measure, of the sensor's current measurements with the prior bathymetry map. Some feasible similarity metrics include cross-correlation (XCOR), normalized cross-correlation (NXCOR), mean absolute difference (MAD) and minimum square distance (MSD) [1]. Due to the nonlinearity of the terrain, it was expected that the probability distribution resultant from the correlation would be multi-modal. TAN filtering methods currently being researched include Kalman-based filtering methods, multi-modal adaptive estimation techniques, and the use sequential Monte Carlo methods, namely point mass and particle filters [1].

In our application of TAN to an AUV, the vehicle built a bathymetry map of its environment using a micro-bathymetry swath sonar sensor. The sonar data was collected onboard the AUV vehicle and then post-processed in a MATLAB environment to "build" a bathymetry map. When the AUV subsequently traversed the same terrain, the new sonar sensor data it was receiving was correlated with the existing bathymetry chart in order to update the vehicle position estimate. Using only sonar data correlations (no state information from the vehicle), this can be an extremely expensive computational process. Therefore, several of the aforementioned methods that effectively fuse the knowledge of the previous vehicle state, the current sonar readings, and the existing bathymetry chart were explored in the scope of this thesis. These methods include the Kalman filter, the extended Kalman filter (EKF), and particle filter. A further glance into the advantages and disadvantages of each of these three methods is covered in Section D, and detailed more explicitly in Chapter IV. A primary motivation behind the eventual selection of the particle filter as a solution to the TAN problem was its ability to accurately estimate the probability distribution of the vehicle state, even when the distribution is multi-modal.

This thesis is the first to address TAN on a small, man-portable AUV. The work is novel in the sense that it works with a bathymetry sonar sensor capable of significantly

higher resolution than most bathymetry sonar systems utilized for TAN. Along with concern to accommodate the higher resolution sensor, initial consideration has been given to image processing techniques and base map generation that are critical in an eventual real-time TAN implementation. This process was validated through simulation on a dataset collected by the AUV.

D.   RELATED WORKS

The technical landscape of TAN methods is only now beginning to reach maturity. Until recently, very few commercial systems employed, or relied significantly upon, any terrestrial sensory information as a component of their navigation. As the field has developed, the TAN method of choice has shifted slightly. In the mid- to late-1990s, TAN methods for AUV's employing Kalman filtering methods were primarily researched and implemented [3]. In particular, due to the aforementioned nonlinearities associated with TAN for an AUV, the extended Kalman filter (EKF) was a favorable method of sensor fusion among researchers. In the early 2000s, particle filters (PF) and point mass filters (PMF) were recognized as approaches well-suited to handle non-linear process and measurement models as well as multi-modal, non-parametric noise distributions. These techniques were selected, in part, due to the rapid increases in computer processing power/capabilities as PF and PMF are computationally expensive algorithms [4]. Several papers published throughout the early 2000s provide empirical support for the superiority of the PF relative to Kalman-based or batch-oriented methods. These papers include Gustafsson [5] in 2001, Nordlund [6] in 2002, and Anonsen and Hallingstad [7] in 2006.

Carreno et al. [1] provide an excellent survey of AUV-based TAN research. Importantly, the survey paper also provides the Bayesian estimation framework relied upon throughout the TAN field. Bayesian estimation is a particularly useful approach in the underwater domain, since it implicitly accounts for the mean and variance associated with the pose of the vehicle. Approaches that use a Bayesian framework include Kalman filtering, multi-modal adaptive estimation and sequential Monte Carlo methods.

The particle filter and point mass filter implementations by Anonsen and Hallingstad [7] on a HUGIN AUV provided very promising results demonstrating the

suitability of recursive Bayesian, sequential Monte Carlo methods to TAN. One large issue that is identified, but not addressed in their approach, is the impact of the terrain "usefulness." Intuitively, flat terrain presents an issue when attempting to correlate the current measurements with the prior map. When the AUV was tested in suitable terrain, both methods yield positional accuracy comparable to their prior map resolution (10 m). However, it was noted that attempts to navigation in poorly suited terrain could often lead to filter divergence.

In 2012, Professors Shane Dektor and Stephen Rock of Stanford completed further testing at Monterey Bay Aquarium Research Institute (MBARI) on the TAN of a Dorado-class AUV [8]. Similar to Teixeira et al. [9] they sought to improve the robustness of the particle filter TAN implementation. Incorrect convergence over time in flat terrain was determined to be a product of "overconfidence" of the filter in estimating position over the featureless terrain. In order to account for the overconfidence, an additional parameter dependent upon terrain suitability was incorporated into the correlation stage of the particle filter algorithm. The parameter effectively scales the observed correlation based upon the usefulness of the terrain being observed, thereby reducing correlation confidence over featureless terrain while maintaining the strong correlation and convergence of the filter over feature-rich terrain.

E.   THESIS ORGANIZATION

The thesis is organized as follows: Chapter II provides a description of the AUV and the sonar used for research. After the system/sensor descriptions, the paper delves into building the bathymetry map necessary in order to conduct subsequent TAN operations. Only after the prior map building methodology is discussed in Chapter III is the selection of a TAN method discussed in Chapter IV. Finally, a dataset is collected and the methodologies described are implemented. The results and conclusions from the testing are presented in Chapter V.

THIS PAGE INTENTIONALLY LEFT BLANK

II. SYSTEM DESCRIPTION

A. REMUS AUV

All data processing and experimental work was completed through the use of a modified REMUS 100 AUV (Figure 1) supplied by the Center for Autonomous Vehicle Research (CAVR) at the Naval Postgraduate School (NPS). The REMUS vehicles are currently designed and manufactured by Kongsberg Maritime (http://www.km.kongsberg.com).

The REMUS 100 in particular is designed for operation in coastal areas in depths of up to 100 meters. This makes the REMUS 100 vehicle versatile in a variety of shallow water mission areas including, from [10]:

- Hydrographic surveys
- Mine counter measure operations
- Harbor security operations
- Environmental monitoring
- Debris field mapping
- Search and salvage operations
- Scientific sampling and mapping

Figure 1.   REMUS 100 AUV onboard CAVR's SeaFox surface vessel

The standard REMUS 100 is a lightweight and compact AUV, weighing approximately 37 kg and having a diameter of 19 cm. Its light weight and manageable size make it easily deployable and recoverable by two-man teams with small boats. The vehicle is modular and can be configured to employ a wide variety of sensors and systems. This includes:

- MSTL side scan sonar
- Upward and downward RDI acoustic Doppler current profiler (ADCP) Doppler velocity log (DVL)
- Undersea acoustic modem
- GPS
- Fore and aft cross-body tunnel thrusters
- YSI-600 Conductivity Temperature and Depth (CTD) sensor
- Optical Backscatter Sensor
- External Power Data Interface

When at the surface, the REMUS 100 vehicle can obtain position fixes using GPS. When underwater, however, the vehicle relies on a long baseline (LBL), ultrashort baseline (USBL) or integrated DVL/GPS/INS Kearfott SeaDeViL navigation solution.

The SeaDeViL system has an advertised navigational uncertainty of 0.5 percent distance traveled circular error probable rate (CEPR) [12]. Essentially, this means that the actual position of the AUV will be within a circle of a radius quantified by 0.5 percent times the distance traveled. The LBL system has a navigational accuracy of ±10 meters and range of 2000 meters. The USBL system has a navigational accuracy of ±1 meter and range of 1500 meters [12].

B.   BLUEVIEW MB2250 SONAR

As mentioned above, the REMUS has a modular external payload configuration. The power data interface provides a nominal 30 volts with an Ethernet and serial connection within a wet-mateable connector. This permits the REMUS AUV to mount forward-looking sensor packages.

The forward-looking sensor package mounted on the NPS REMUS AUV for the data collected in this thesis is equipped with a BlueView 900 KHz forward-looking sonar and a BlueView 2250 KHz downward-looking, ultra-high resolution sonar. Both systems are blazed array sonars. A blazed array sonar system employs methods similar to echelette diffraction gratings in optics in order to turn a single sonar acoustic signal into a swath of sound beams [13]. Each beam is diffracted at a different frequency and therefore at a different angle relative to the source. The size and shape of each beam is dependent upon the frequency band of the original sound source as well as the shape of the stave diffracting the sound. Figure 2 shows the magnitude and direction of each beam of a composite blazed array sonar along with the frequency range.
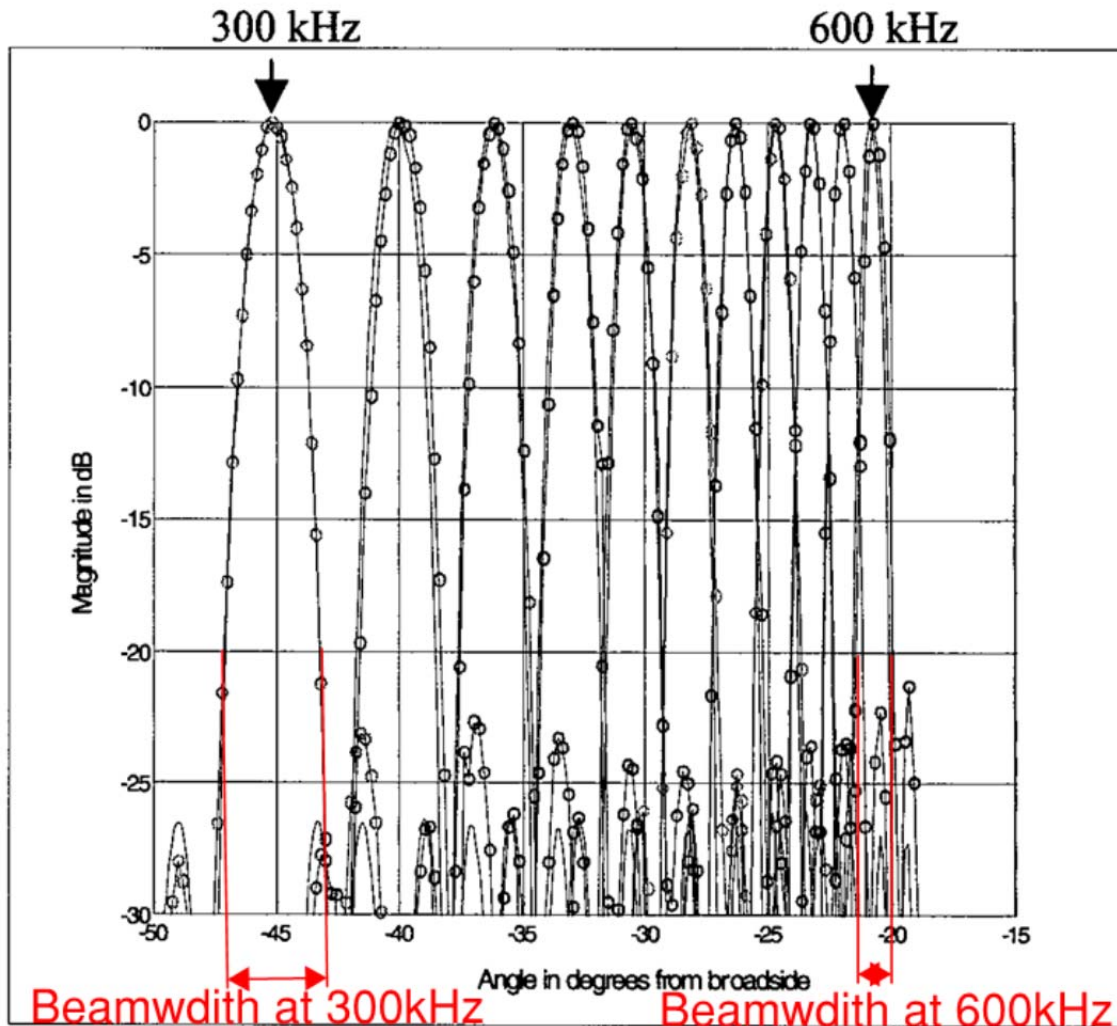
Figure 2.   Composite blazed array sonar beam magnitude and direction for
frequencies between 300 kHz and 600 kHz, from [13]

As can be seen, the lower frequencies create larger beams and as the frequency increases, the beam size decreases. The frequency to spatial angle relationship remains consistent throughout the process. Therefore, once the sound from each beam reflects back towards the sonar system, the process is reversed and the individual beams are merged back into a single signal [13]. Due to the directionality of the individual beams, a wide swath of coverage can be attained with a high level of accuracy. For these reasons, most bathymetry mapping missions utilize a form of a blazed array sonar system.

Table 1 provides the specifications of the 2250 KHz downward-looking, ultra-high resolution sonar used as the primary sensor in this thesis.

10

Table 1.   BlueView MB2250 sonar specifications, after [14]

Attribute	Value
Field of View	45º x 1º
Minimum Range	0.5 meters
Maximum Range	10 meters
Beam Width	1º x 1º
Number of Beams	256
Beam Spacing	0.18º
Time Resolution	0.39 inches (0.01 m)
Max Update Rate	40 Hz
Frequency	2.25 MHz

THIS PAGE INTENTIONALLY LEFT BLANK

III. MAP BUILDING

The first step in the TAN process is the development of a base reference map. It is this map that is compared with bathymetry sensor measurements to determine the best correlation to determine the best position estimate for the AUV. This chapter describes the challenges and necessary steps for building the base bathymetry map.

A.   BATHYMETRY MAP BUILDING

Constructing an accurate bathymetry map involves the following considerations.

- AUV kinematics and dynamics and environmental impact
- Limited sonar range
- Low and asymmetrical frequency of sonar pings
- Computational power constraints
- Data storage constraints
- Inherent inaccuracies associated with uncertain INS pose estimations

One of the most challenging aspects of accurate map building is accounting for the positional uncertainty of the vehicle collecting the micro-bathymetry sonar images. Any navigational aid that can be utilized in order to constrain or reduce the uncertainty of the AUV is desired. This includes GPS, LBL and USBL systems.

The growing, unconstrained uncertainty associated with the INS is by no means nominal. A conventional navigation pattern for complete sensor coverage is often called a "navigate by rows," or "lawnmower," mission. In the case of the REMUS vehicle, a typical survey area may be approximately 400 meters by 400 meters. Through setting the desired altitude of the vehicle at 9 meters, and given that the beam from the micro-bathymetry sonar is 45 degrees wide, the sonar swath will be 10.04 meters wide by the time it reaches the seafloor. Therefore, through using a spacing of 10 meters between each row, complete sensor coverage can be attained in ideal circumstances. In total, the AUV will travel approximately 16,800 meters. Given that the positional uncertainty is equal to 0.5 percent of the distance traveled without the use of any external navigational aids, the accumulated uncertainty by the end of the mission is 84 meters CEPR.

Figure 3 provides a visual representation of the accumulation of uncertainty as a mission progresses. The blue dots represent the mean estimate of the filter and the red ellipses represent the positional uncertainty associated with the INS navigation solution. Note that the positional uncertainty is drawn such that there is a 50 percent chance that the true position of the AUV is somewhere within the boundary.

Mission parameters such as vehicle altitude, speed, and tightness of turns should also be given due diligence. A higher altitude off the seafloor inherently provides increased coverage area and thus lessens the needed distance traveled by the AUV in order to survey a specified area. The altitude is limited by the range of the sonar sensor (10 meters) plus a slight buffer of one to two meters in order to ensure abrupt changes in the topography do not cause a loss of bottom coverage. Similarly, given that the sonar system pings at roughly 1 Hz, additional coverage can be gained by decreasing the speed of the vehicle. Lastly, the dynamics and kinematics of the vehicle should be kept in mind in order to appropriately set realistic mission paths (i.e., turns wide enough that the vehicle is capable of making, or to set the minimum speed at which the vehicle should operate in order to maintain its depth and overall controllability).
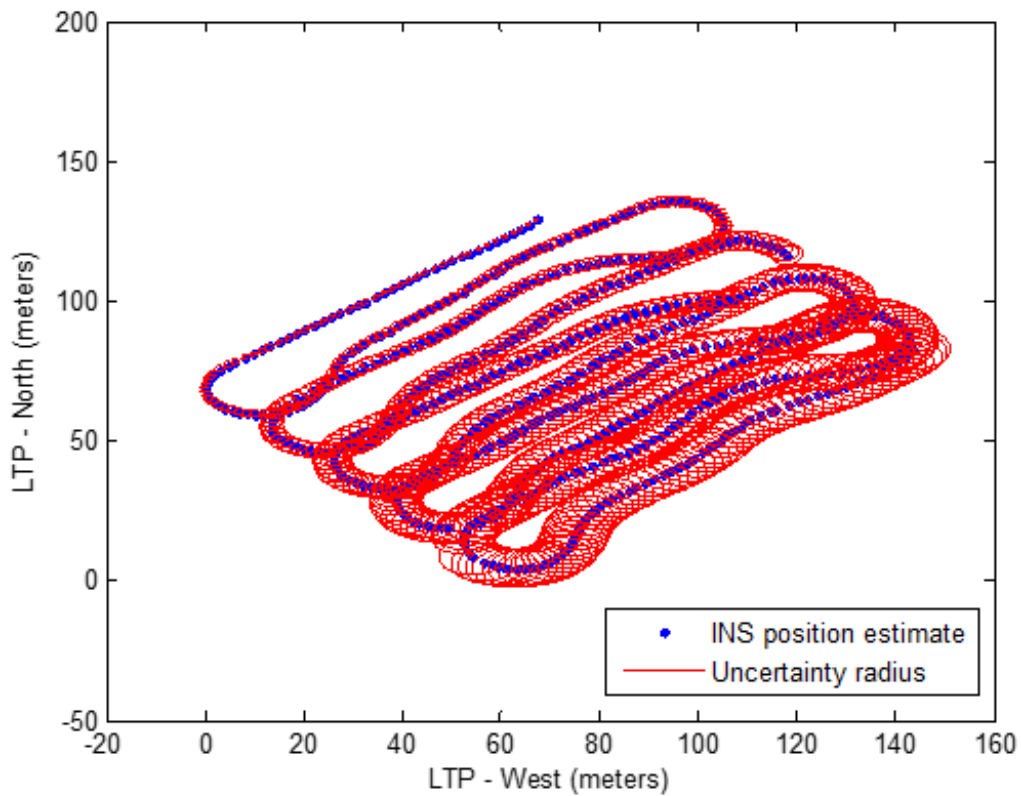
Figure 3. REMUS AUV mission route with uncertainty—first navigate rows objective

Figure 4 clearly quantifies the accumulation of navigational uncertainty throughout the course of the mission. The REMUS vehicle embarks on the mission with a GPS fix providing accuracy to within three meters. Approximately midway through the mission, the REMUS vehicle surfaces again in order to obtain another GPS fix. The GPS improves the INS solution and again confines the estimated position to a three-meter radius area.
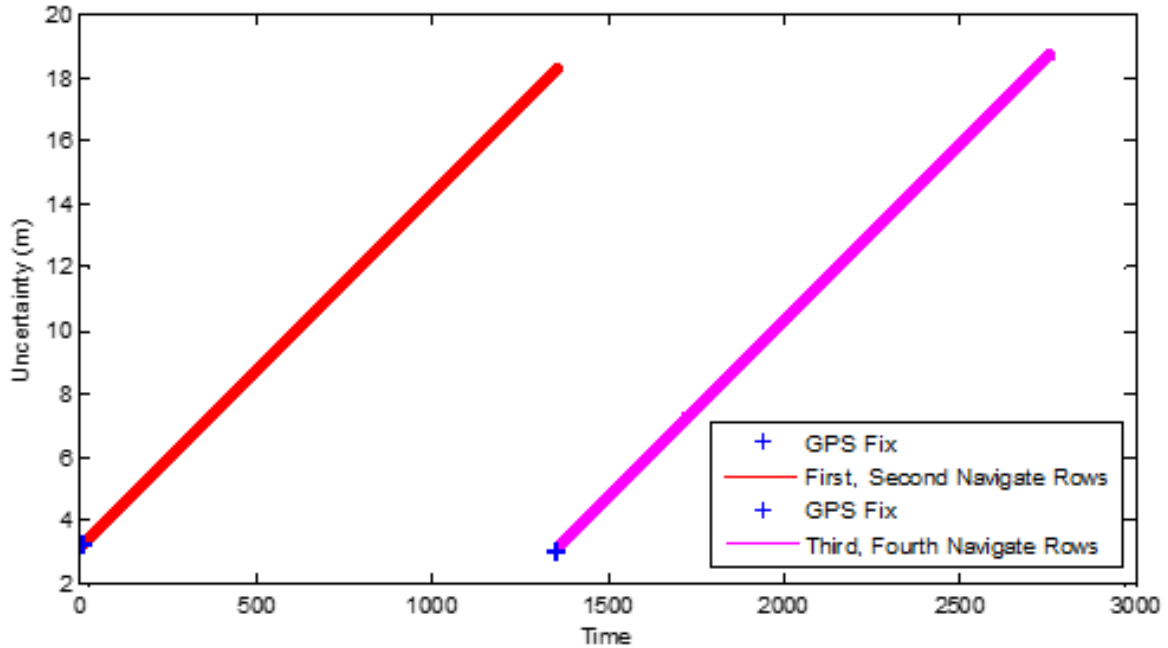
Figure 4.   Accumulation of REMUS positional uncertainty with GPS update

Upon the completion of the mission, a final GPS fix is obtained and the positional uncertainty is constrained once again. It is clear from Figures 3 and 4 above that the vehicle must either surface periodically for a GPS fix or navigate its track with the aid of an acoustic navigation system in order to maintain a reasonable position estimate. Alternatively, the micro-bathymetry surveying may be completed using a surface vessel. This way, the vessel would have persistent GPS coverage. However, this method has its own limitations. For example, the high resolution BlueView MBE2250 sonar used in our experiments would severely constrain the operating area and coverage of the surface vessel due to its limited range. Typically, a sonar operating at a much lower frequency would be used in order to increase the sonar range. Using a lower frequency, however, negatively impacts the sonar image resolution.

B.   SONAR IMAGE PROCESSING

Over the course of a mission, the AUV collects sonar images from its onboard sonar sensor. In a real-time implementation, image-processing techniques are applied onboard the AUV to provide a series of altitude measurements. For this thesis, the

analysis was conducted via post-mission processing. Upon completion of the mission, the raw images are then imported from the vehicle into a MATLAB environment in order to be post-processed. The goal of the sonar image processing step is to identify and extract information regarding the topology of the seafloor surveyed.

A typical raw sonar image from the BlueView MB2250 micro-bathymetry sonar is shown in Figure 5.
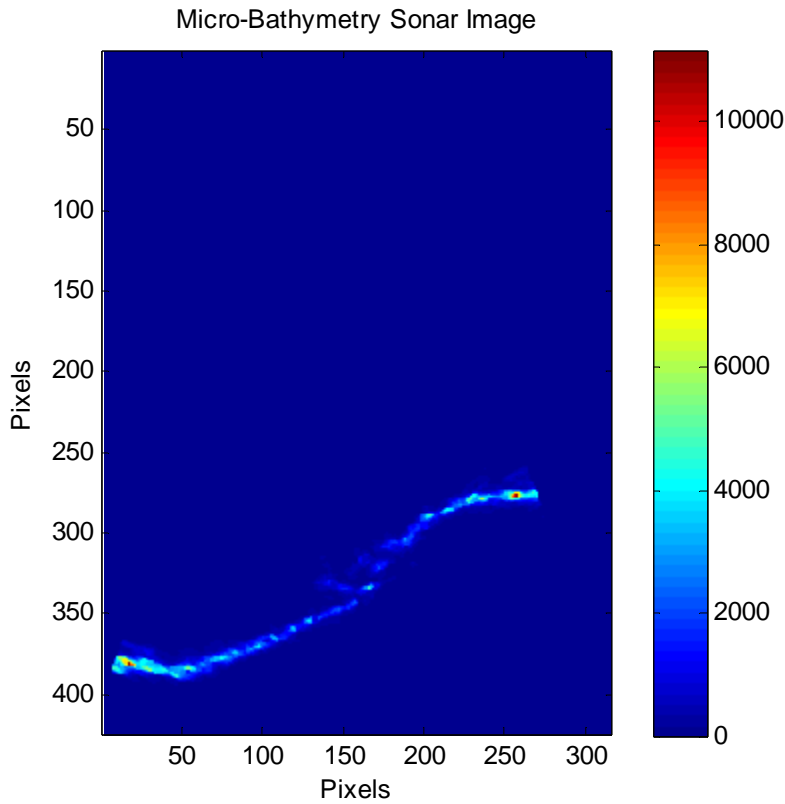
Figure 5.   Sample micro-bathymetry sonar image

The intensity values of the image vary from 0 to 10000. A threshold of 125 was determined empirically to be a suitable threshold for separating noise from actual bottom returns. Thresholding attempts to minimize false acceptances of noise as actual bottom returns while also minimizing false rejections, where valuable bottom information may be discarded as noise. It should be noted here that the thresholding value of 125 is the result of an empirical evaluation of a particular data set. It would be useful to include an

autonomous methodology for determining a filtering threshold regardless of the operational environment (i.e., sandy or muddy ocean floor). An adaptive thresholding method is a consideration for future work. For the dataset collected for this thesis, a max return of every eleventh column can be located in the image and compared with a threshold value of 125. If the maximum pixel value of the column is above 125, it is regarded as the bottom location in the image. Based upon sampling every eleventh column, a bottom return can be provided approximately every 0.25 meters. A map resolution of 0.25 meters was determined appropriate in seeking to accomplish the objectives set in this thesis. In future work, if determined desirable, the resolution could be increased to the fundamental 0.023052 meters/pixel associated with the sonar images produced. An example of finding the max return of each eleventh column in the sonar image is depicted in Figure 6.
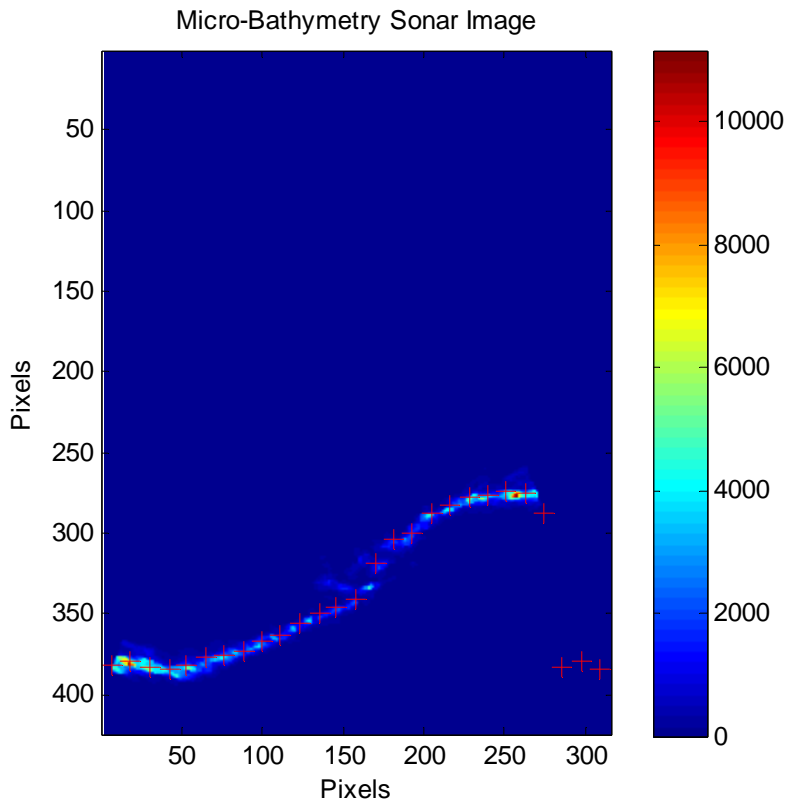
Figure 6.   Sample sonar image with max returns

In the example of Figure 6, the four red pluses to the right of the visible bottom returns would be removed by the threshold from the collection of useful bottom data. The final set of data points collected would be those represented by the red pluses in Figure 7. Using the pixel location of each point greater than the threshold along with the associated conversion of 0.023052 meters per pixel, the distance in meters to each max return can be computed in the vehicle's local frame.
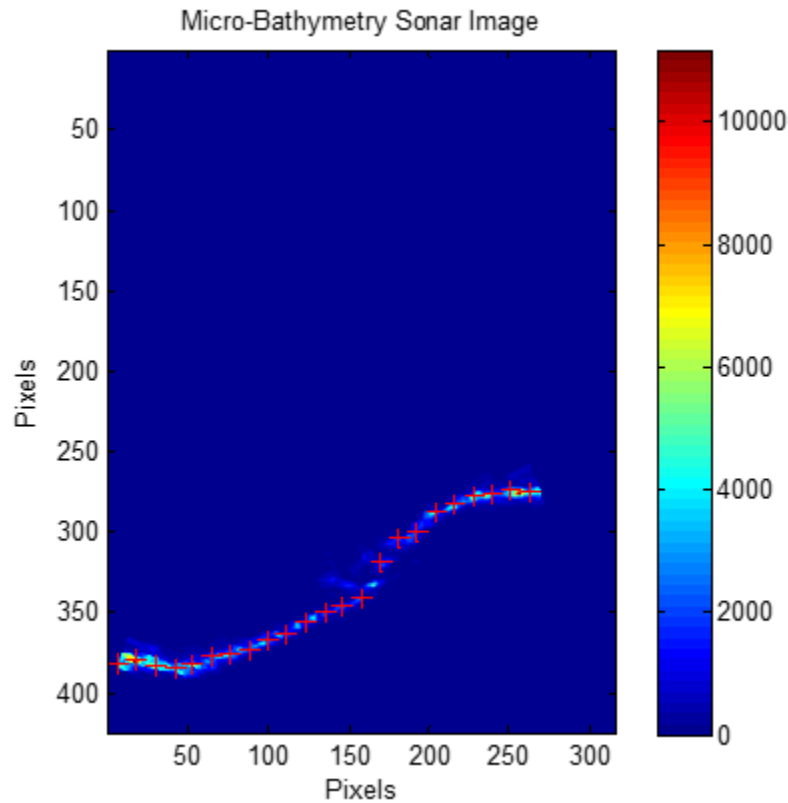
Figure 7. Sonar image with max returns after thresholding

C. TRANSFORMATION TO GLOBAL FRAME

Since the BlueView MB2250 sonar is rigidly attached to the underside of the REMUS 100 AUV, each sonar image is captured relative to the body's pose. In order for the information to be useful, the bottom returns must all be represented in the same global map. The rotation transformation converts the identified bottom locations in the body frame to bottom locations in the local tangent plane (LTP) and converted into the global

frame. First, the vehicle's pose is taken into account. The location of the bottom returns is affected by both the vehicle's roll, pitch and yaw, represented by ϕ, θ, and ψ respectively. The Euler angle rotation matrix that rotates the information from the body to LTP frame is shown in equations (1) and (2).

$$R_{Body}^{LTP} = R_{x,roll} R_{y,pitch} R_{z,yaw} = \begin{pmatrix} 1 & 0 & 0 \\ 0 & \cos(\phi) & -\sin(\phi) \\ 0 & \sin(\phi) & \cos(\phi) \end{pmatrix} \begin{pmatrix} \cos(\theta) & 0 & \sin(\theta) \\ 0 & 1 & 0 \\ -\sin(\theta) & 0 & \cos(\theta) \end{pmatrix} \begin{pmatrix} \cos(\psi) & -\sin(\psi) & 0 \\ \sin(\psi) & \cos(\psi) & 0 \\ 0 & 0 & 1 \end{pmatrix} \quad (1)$$

$$R_{Body}^{LTP} = \begin{pmatrix} \cos(\theta)\cos(\psi) & \sin(\phi)\sin(\theta)\cos(\psi)-\cos(\phi)\sin(\psi) & \sin(\theta)\cos(\phi)\cos(\psi)+\sin(\phi)\sin(\psi) \\ \cos(\theta)\sin(\psi) & \sin(\phi)\sin(\theta)\sin(\psi)+\cos(\phi)\cos(\psi) & \sin(\theta)\cos(\phi)\sin(\psi)-\sin(\phi)\cos(\psi) \\ -\sin(\theta) & \sin(\phi)\cos(\theta) & \cos(\phi)\cos(\theta) \end{pmatrix} \quad (2)$$

All bottom returns from the micro-bathymetry sonar are collected in the AUV's *x, y,* and *z* directions, using the conventional body-fixed coordinate system abiding by the right hand rule. In order to express all data points as relative to the ocean surface, the depth of the AUV must be added to the new *z* direction of the data points. The origin of the LTP is defined as a point on the surface of the ocean, and therefore a transformation between the vehicle's body-fixed frame and the LTP necessitates both a rotation and translation of the reference frame. The rotation is determined by the vehicle Euler angles while the translation is determined by vehicle depth and an arbitrary *x, y* origin. An example of an AUV on a bathymetry mapping mission is shown in Figure 8.
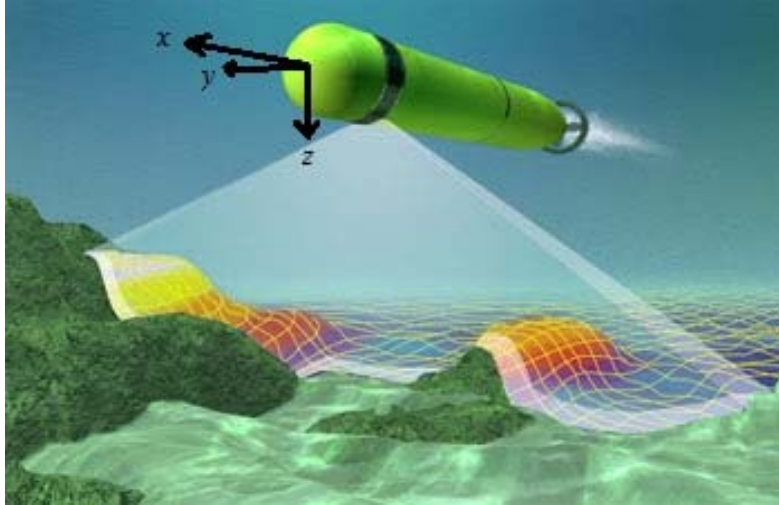
Figure 8.   AUV with visible bathymetry sonar overlay, after [15]

In practice, the body-fixed coordinate frame would originate at the vehicles center of gravity. The positioning of the coordinate frame in Figure 8 serves solely as a visual guide for the reader. Figure 9 depicts the very same image as Figure 8, but with red crosses symbolizing the maximum sonar returns associated with the seafloor.
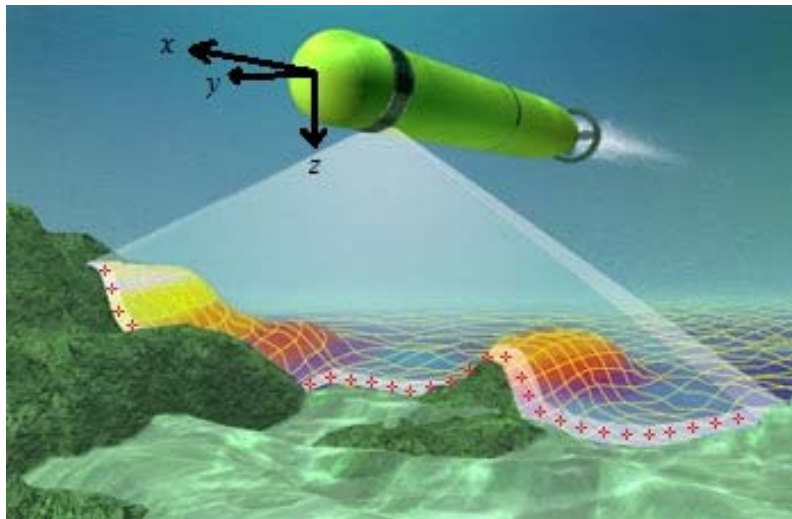
Figure 9.   AUV with visible bathymetry sonar overlay and maximum bottom returns, after [15]

The coordinates of each red cross is first expressed relative to the vehicles body frame. After rotation and translation to the LTP, the same sonar returns seen in Figure 9 would look approximately like the data points plotted in Figure 10.
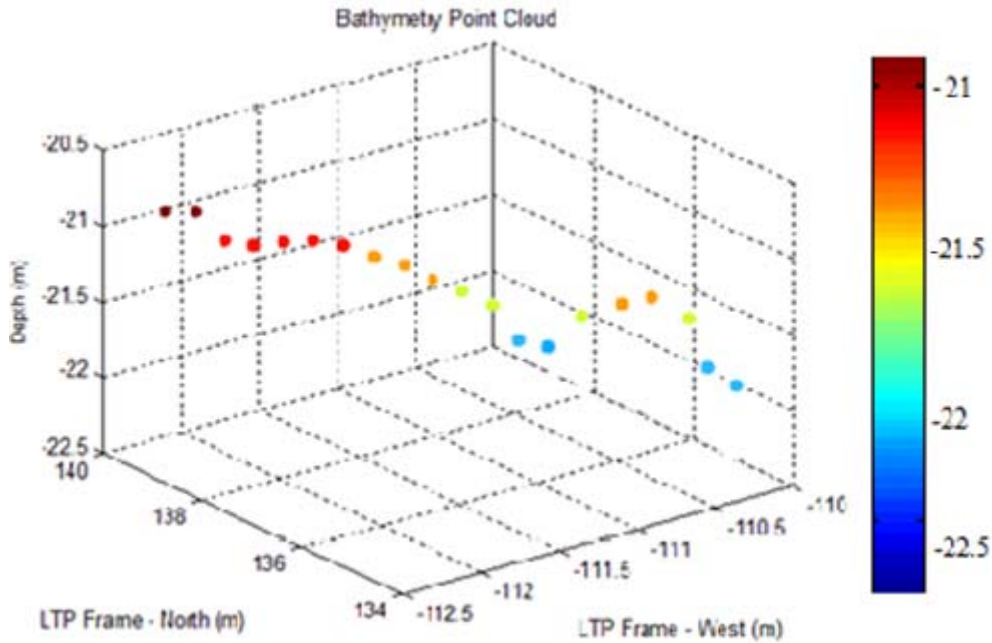
Figure 10.   Example sonar bottom returns expressed in LTP

Since the AUV mission conducted for this project typically did not transverse more than several hundred meters across the seafloor in any direction, the LTP reference frame supports an acceptable representation of the data. Nonetheless, the points are also available represented in the global frame through latitude and longitude. The transformation from the LTP frame to the global frame was completed using MATLAB's Map Toolbox.

D.   CONSTRUCTING THE BATHYMETRY MAP

Once the entire set of data for the mission was transformed into the global reference frame in latitude and longitude, all of the points can be displayed coherently as a point cloud in 3D space. An example of several successive data points being displayed simultaneously in the LTP frame is shown in Figure 11.

22
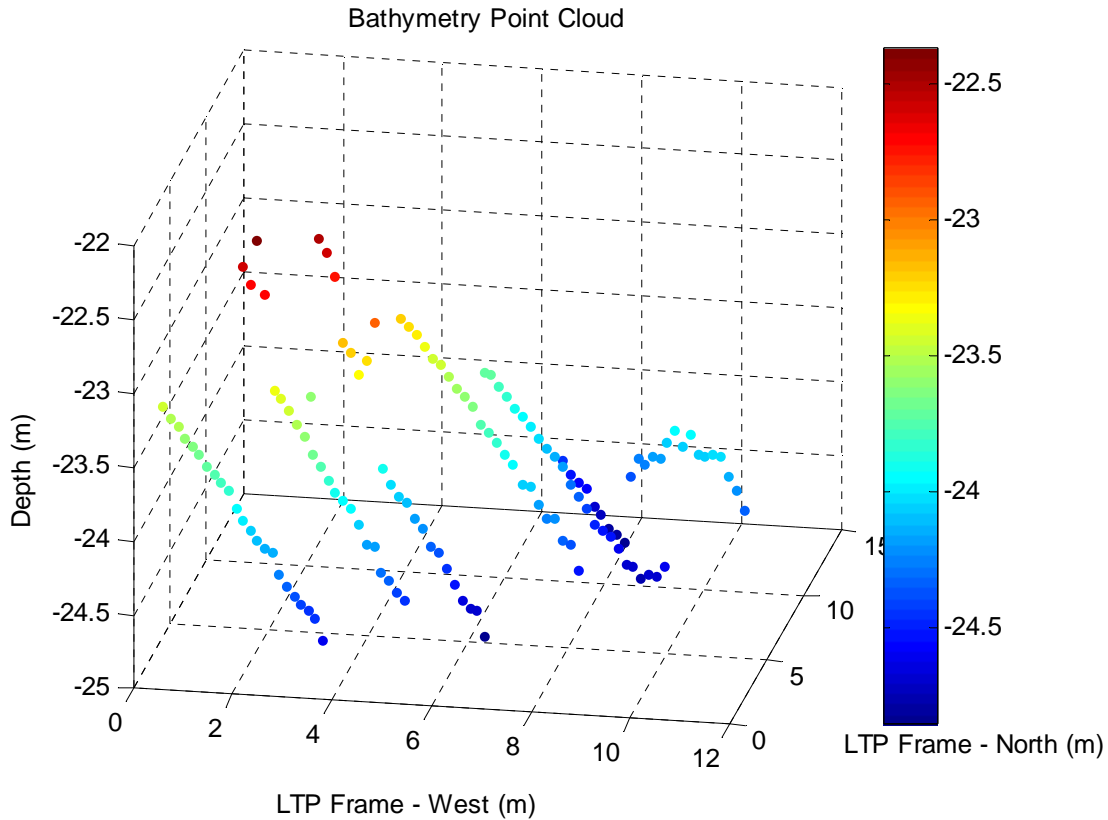
Figure 11.   Several successive sonar pings displayed together in the LTP frame

During the correlation steps a sonar ping is rotated and translated into the LTP and compared with the base bathymetry map. The base map will likely not have complete coverage due to limited sonar resolution, AUV path planning and following constraints, and/or a slow sonar ping frequency among other reasons. A lack of complete coverage may result in an inability to make a comparison between the sonar ping and the base map as the sonar ping may ensonify an empty region in the base map. There are a number of possible approaches for handling the sparse data; however, this thesis provides complete coverage to a desired resolution using linear interpolation. The linear interpolation was performed in the MATLAB environment with the built in *TriScatteredInterp* function. The resultant surface passes through every data point in the set and linearly interpolates between neighboring data points. A basic linear interpolation may not best represent the

underlying topography and further research may be done in this area to identify a better-suited method of data interpolation. The linear interpolation of the sonar pings displayed in Figure 11 is exhibited in Figure 12.
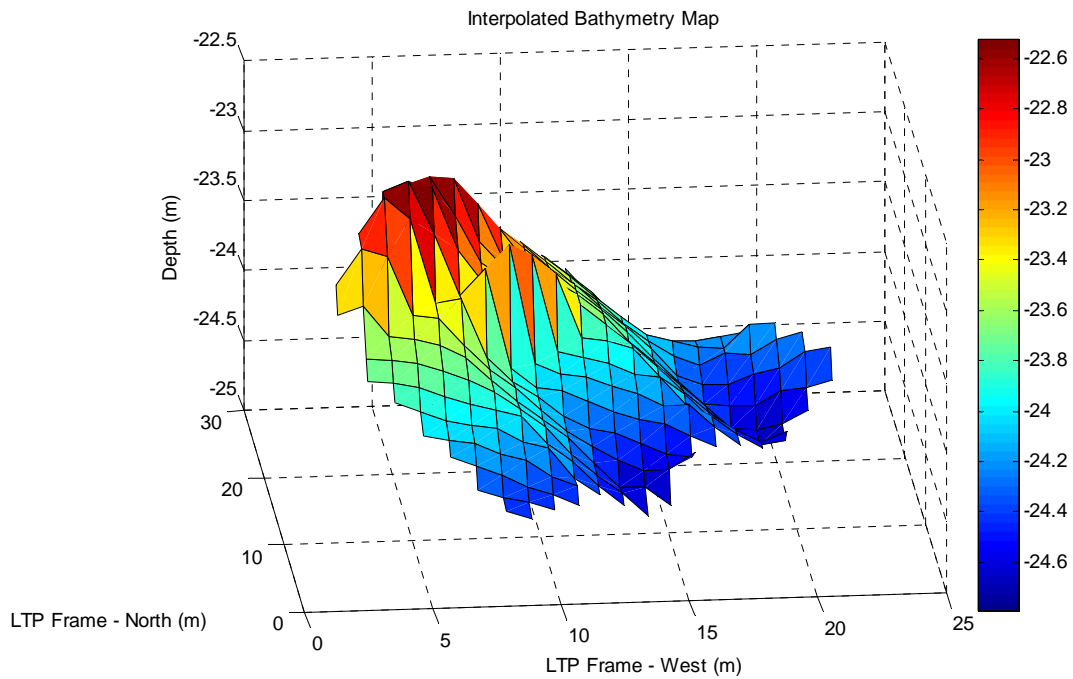
Figure 12.   The linear interpolation of the sonar pings from Figure 11

The same linear interpolation is applied to all data points collected within the survey area of the REMUS AUV. As one would assume, the linear interpolation better approximates the underlying topography in regions with a higher density of data points and is less accurate the sparser the data is.

# IV.   TERRAIN AIDED NAVIGATION

This chapter addresses an optimal estimation approach to TAN. The goal is to use the prior bathymetry map from Chapter III as an aid to vehicle navigation. Therefore, the chapter starts with identifying a process and measurement model for the vehicle. The process and measurement model will be vital in the latter steps of filtering the positional estimation of the vehicle. Next, the correlation methods that quantify the similarity between the prior map and each new sonar ping are discussed and a method is selected. The correlation method coincides with the measurement model. Finally, the prior three components work together within the domain of a recursive Bayesian filtering method in order to estimate the vehicle state. Both Kalman-based filters and particle filters are discussed, and advantages / disadvantages for each are noted. Consistent with recent literature, and taking into consideration the nonlinearities and multi-modalities inherent to the TAN problem, a particle filter was chosen to be implemented.

A.   PROBLEM STATEMENT

1.   Process Model

A generalized process model for an AUV is shown in equation 3, first proposed by [8].

$$x_{k+1} = x_k + \delta x_k^{INS} + r_k \tag{3}$$

where x_k is the vehicle's x, y, z position in the LTP and r_k is representative of INS noise. The INS noise is assumed to be a zero-mean, white noise.

2.   Measurement Model

The sonar and map models are shown in Equations 4 and 5 respectively [8]. The map and sonar errors, $e_{i,k}$ and υ_{map} are treated separately. Therefore, the sensor model uses the difference between the true terrain for the ith ping at time k and the measured altitude for the ith ping at time k along with a range dependent error, $e_{i,k}$, in order to

determine the range $y_{i,k}$. The map model essentially states that the true terrain range $h(x_k)_i$ differs from the expected range $\hat{h}(x_k)_i$ by an error υ_{map}.

$$y_{i,k} = z_k - h(x_k)_i + e_{i,k} \tag{4}$$

$$\hat{h}(x_k)_i = h(x_k)_i + \upsilon_{map} \tag{5}$$

- z_k is the vector of the measured altitudes at each sonar ping.

- $y_{i,k}$ designates the ranges associated with the ith ping at time step k

- $h(x_k)_i$ is the true terrain range for the ith ping at time k

- $\hat{h}(x_k)_i$ range from a priori map

- $e_{i,k}$ range dependent error $\quad e_{i,k} \sim N(0, \sigma^2_{i,k,sensor})$

- υ_{map} map error $\quad\quad\quad\quad \upsilon_{map} \sim N(0, \sigma^2_{map})$

Since the position of the AUV is not known precisely and the map has inherent errors, $h(x_k)_i$ is not known. Therefore, effectively our goal with TAN is to minimize the argument $y_{i,k}$ by varying $\hat{h}(x_k)_i$ throughout the search area.

3.   Correlation Method

At each time step in the recursive algorithm, the altitude data from the micro-bathymetry sensor is compared to the prior bathymetry map at several locations. A correlation technique is necessary between the sensor data and the bathymetry map to quantify the similarity between each such that the best correlation is selected as the most probable location of the AUV. The correlation method should be robust across varying levels of depth as well as to sensor noise. Overall, the difficulties associated with map correlation are largely consistent with those of building the map originally. One of the significant difficulties associated with TAN is the low and asymmetric frequency of ping information.

Several different methods of correlation were tested including cross-correlation (XCOR) [16], normalized cross-correlation (NXCOR) [16], mean absolute difference (MAD) [1], a normalized minimum absolute difference, and a mean square difference (MSD) [1].

$$XCOR(x_t) = \frac{1}{N} \sum_{i=1}^{N} \left(z_{t,i} - h_i(x_t) \right) \tag{6}$$

$$NXCOR(x_t) = \frac{\sum_{x,y} \left[f(x,y) - \overline{f}_{u,v} \right] \left[t(x-u, y-v) - \overline{t} \right]}{\left\{ \sum_{x,y} \left[f(x,y) - \overline{f}_{u,v} \right]^2 \sum_{x,y} \left[t(x-u, y-v) - \overline{t} \right]^2 \right\}^{0.5}} \tag{7}$$

$$MAD(x_t) = \frac{1}{N} \sum_{i=1}^{N} \left| z_{t,i} - h_i(x_t) \right| \tag{8}$$

$$MSD(x_t) = \frac{1}{N} \sum_{i=1}^{N} \left(z_{t,i} - h_i(x_t) \right)^2 \tag{9}$$

In comparison testing with each method, NXCOR, MAD, and MSD all performed similarly well. XCOR was determined to be ill-suited to the problem as the correlation performed is not scale invariant, meaning the actual depth values from the prior map influence the result of the correlation. This is dangerous, as the correlation value between a sonar ping and itself may actually be poorer than a correlation between the same ping and an arbitrarily high valued set of sonar data. NXCOR successfully addresses this undesired dependence upon scale. The main downfall of NXCOR, however, was that the implementation only recovers Cartesian shifts in data. The MAD and MSD implementations, on the other hand, can recover rotation shifts as well as translational shifts. Both MAD and MSD performed similarly well, but due to the nature of squaring the differences, MSD exaggerates the peaks and valleys of the correlation matching. Therefore, MAD was chosen in order to avoid this sort of "overconfidence" in the correlation result.

The output of the correlation step is a matrix equivalent to the size of the area of uncertainty searched. In the case of the MAD and MSD implementations, each cell's value is the result of the correlation between the new ping and the prior map at that location. Through performing an element-wise inversion of each cell and then normalizing the whole matrix so that the sum of the matrix is equal to 1, a probability density function describing the probability of sensing the current ping information given

27

the AUV position in the map is calculated. This probability density function is key to the measurement update steps in the subsequent sections.

4.   Bayesian Methods

As previously stated, given the dead reckoning nature of navigating by INS, there is a growing uncertainty associated with the vehicle's pose over time. Clearly then, the TAN problem is best expressed through a stochastic process. Thus, the x_k used in the process model of part 1 is not a single, precise *x, y, z* location, but a stochastic variable representing the estimate of the position. The well-known Bayesian filter represents a broad framework for which to estimate the *a posteriori* probability distribution of the vehicle's state given a process model, measurement model, and the *a priori* probability distribution of the state. The Bayesian filter is represented in equations 10 and 11 as consisting of a prediction and correction step. The prediction determines the probability of the vehicle being at state x_k given all of the previous measurements. This is done using the state transition model, represented by $p(x_k | x_{k-1}, u_k)$, and the a priori probability distribution $p(x_{k-1} | D_{k-1})$. The correction step then uses the result of the prediction step, along with the current measurement probability given the current state, represented by $p(y_k | x_k)$, and the probability of the measurement given all the previous measurements, represented by $p(y_k | D_{k-1})$.

$$PREDICTION : p(x_k | D_{k-1}) = \int p(x_k | x_{k-1}, u_k) p(x_{k-1} | D_{k-1}) \tag{10}$$

$$CORRECTION : p(x_k | D_k) = \frac{p(y_k | x_k) p(x_k | D_{k-1})}{p(y_k | D_{k-1})} \tag{11}$$

$p(x_{k-1})$ Probability of robot at certain state (pose) at time step *k*-1

$p(x_k | x_{k-1}, u_k)$ State transition probability (motion model)

$p(y_k | x_k)$ Measurement probability - Probability of observing y_k when at

state x_k

28

$$D_k = \{y_i : i = 1, ..., k\} \quad D_k = \{y_i : i = 1, ..., k\} \quad \text{Set of all measurements up until time } k$$

The Bayesian filter above provides the general framework for which state estimation occurs. The Bayesian filter cannot be used directly; however, as there is not an analytical solution to the equations. Instead, recursive solutions to the Bayesian filter, such as the Kalman filter and particle filter, are potential methods for solving the Bayesian estimation problem.

B. EVALUATION OF RECURSIVE BAYESIAN ESTIMATION METHODS

The recursive Bayesian estimation methods that were evaluated in the context of this thesis were the Kalman-based methods as well as particle filtering. First, a brief summarization of the Kalman filter is provided.

The Kalman filter relies upon a linear system of differential equations, typically expressed in state-space format as in equations 12 and 13, from [17].

$$x_k = Ax_{k-1} + Bu_{k-1} + w_{k-1} \tag{12}$$

$$y_k = Hx_k + v_k \tag{13}$$

Time update (prediction)

$$\hat{x}_k^- = A\hat{x}_{k-1} + Bu_{k-1} \tag{14}$$

$$P_k^- = AP_{k-1}A^T + Q \tag{15}$$

Measurement Update (correction)

$$K_k = P_k^- H^T \left(HP_k^- H^T + R \right)^{-1} \tag{16}$$

$$\hat{x}_k = \hat{x}_k^- + K_k \left(y_k - H\hat{x}_k^- \right) \tag{17}$$

$$P_k = \left(I - K_k H \right) P_k^- \tag{18}$$

where:

P_k —A posteriori error covariance matrix

P_k^- —A priori error covariance matrix

Q —Process noise covariance matrix

R —Measurement noise covariance matrix

K —Kalman gain

w_{k-1} —Zero mean, white process noise $\sim N(0, Q)$

v_k —Zero mean, white measurement noise $\sim N(0, R)$

As partially evidenced by its formulation, the Kalman filter requires linear and Gaussian assumptions. The EKF has a largely similar representation; however, it is able

29

to complete the prediction step of the filter using a nonlinear set of differential equations. Therefore, the EKF is typically a better estimator than the Kalman filter for problems governed by a nonlinear process and/or measurement model. Nonetheless, the EKF still linearizes about the current mean and covariance at each time instance and requires the same Gaussian assumptions as the ordinary Kalman filter [17].

The particle filter is a different form of recursive Bayesian filtering. The particle filter discretizes the continuous probability density functions associated with Bayesian filter through a large set of particles [1], [18]. Each particle represents a potential state. The particles are distributed roughly according to the *a priori* and *a posteriori* probability density functions. As each particle represents a potential state of the vehicle, each particle is passed through a recursion of propagation (according to the process model) and measurement updates. The algorithm for a commonly used particle filtering method called a sequential importance resampling (SIR) particle filter, is shown in Figure 13.

1) Initialize - Approximate the a priori probability by a discrete number of equally weighted particles

2) Collect new observation / measurement

3) Compute importance weight according to the probability of observation given particle's state

4) Normalize particle weights

5) Resample from particles according to weights (each new particle is equally weighted)

6) Propagate each particle to next time instance using process model

7) Repeat steps 2-6

Figure 13.   SIR particle filter algorithm, after [19]

The initialization of the particle filter is essentially a discretization of the probability density function at that time. In the case of the REMUS vehicle, an

initialization of the particle filter would be performed upon diving and would be based upon the uncertainty associated with the GPS fix just prior to diving. The next main step in the algorithm is related to the measurement update. The measurement update is performed by collecting the new measurement and weighting each particle according to the probability of being at that particular state given the new measurement. The weights for all particles are then normalized. Next is the resampling step. The same number of particles are drawn from the weighted particles, but are once again equally weighted. Once the particles have been resampled, the process model is used to propagate the particles forward to the next time instance. The filter then continues on to collect another measurement, weight the particles accordingly, resample, and propagate the particles for each time step. These steps can be done in real-time as the measurements/observations are being received. If there are no measurements at a given time instance, the particles are still propagated with the process model until a new measurement is available.

One of the most advantageous aspects of particle filtering, especially with consideration to TAN for an AUV, is that it does not make any assumptions on the system model. While even the EKF makes certain linear and Gaussian assumptions, particle filter implementations do not. With a sufficient number of particles, nonlinear and multi-modal systems models can still be well-approximated. The main disadvantage of particle filters in comparison with Kalman-based filters is the significant increase in required computational processing power. Increased processing power is needed for particle filtering as typically 1,000–10,000 particles are required for an accurate approximation to the state probability density function [1]. Each particle must be propagated and updated at each time instance, and therefore computational demand can be significant.

C. SELECTION AND APPLICATION OF METHOD

Both Kalman-based methods and particle filters rely partially on measurement updates. In terms of AUV TAN, the measurements are the depth of multiple points on the seafloor beneath the vehicle. As terrain in general can vary greatly, with various mountains, valleys, peaks and dips, the measurements collected are highly nonlinear.

31

With such nonlinearity associated with the measurements, it is typically unclear exactly where within a region of terrain any single measurement may have come from. In other words, when correlating the measurements collected from a single ping with a prior map, especially given sensor and map error, there are likely multiple areas within the region that seem to correlate well. Over time, however, one such positional estimate will continue to correlate well while the others will not. It is due to the nonlinearity associated with terrain measurements and the resultant multinomial probability distributions that particle filtering was implemented vice a Kalman-based method. An example of the probability density function output from the correlation, or measurement update step, has been taken from a dataset described in the Chapter V results and is shown in Figure 14. Clearly, the distribution in the example of Figure 14 is binomial. With the potential for such multinomial distributions in mind, the particle filter was the preferential choice for filtering.
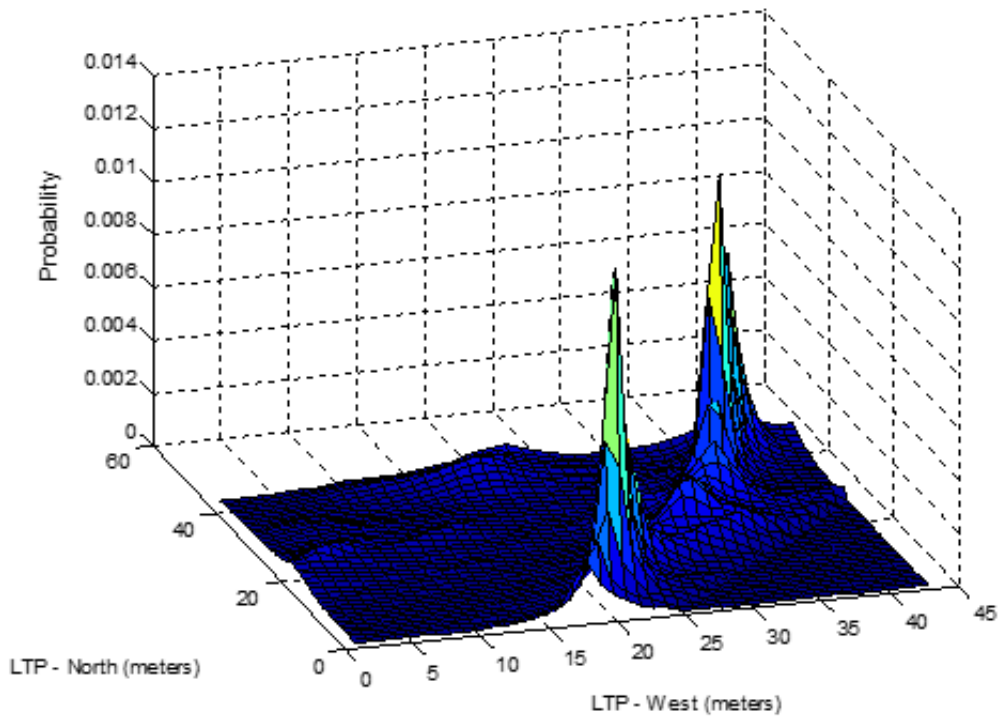

Figure 14.   Probability of measurement given state— $p(y_k \mid x_k)$

The sequential importance sampling (SIS) particle filter formed the foundation for most particle filters developed since [18]. The SIR particle filter is a later derivative of the SIS particle filter that differs in one key aspect; the resampling step. Through resampling, the particle filter can avoid a documented degeneracy phenomenon, where after a few iterations all particles have negligible weights except for one. Resampling essentially eradicates particles with small weights and instead concentrates on particles with larger weights. Additionally, the SIR particle filter requires minimal assumptions beyond the knowledge of the state dynamics and measurement functions [18]. The simplicity, popularity [1], and avoidance of the degeneracy phenomenon were key influencing factors in the decision implement the SIR particle filter as a TAN filtering method.

THIS PAGE INTENTIONALLY LEFT BLANK

V. EXPERIMENTATION

A. DATA SET COLLECTION—SEATEST II

The primary source of data used for this thesis originates from cooperative experimentation entitled "SEATEST II." The mission was conducted as a part of a joint experiment between CAVR at NPS and the NASA Johnson Space Center (JSC). The overarching goal of the collaboration with the JSC was to quantify the effects of autonomy on mission effectiveness, efficiency, and safety for joint robot-human operations [20].

The platform from which the cooperative experimentation took place is the Aquarius Underwater Research Station located in Islamorada, Florida. The Aquarius underwater research habitat is the only operational underwater habitat in the world and is operated by Florida International University (FIU). SEATEST II is similar to a series of exercises collectively known as NASA Extreme Environment Mission Operations (NEEMO) where astronauts train in the undersea habitat as an analogue to space operations. These "aquanauts" may be station at Aquarius for as long as a month at a time. The area of operations is visually represented by the Google Earth screenshot in Figure 15.
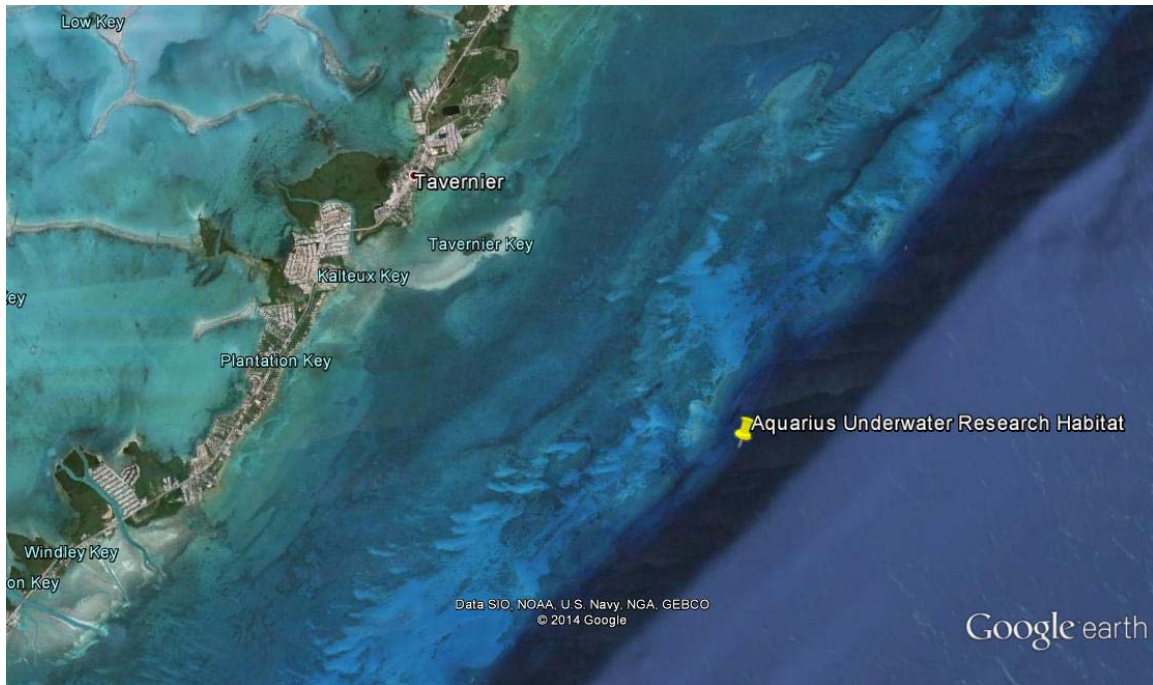
Figure 15.   Aquarius Research Station—Coast of the Florida Keys, from [21]

CAVR contributed to the research effort with two REMUS 100 AUVs and a SeaBotix vLBV300 Tethered, Hovering AUV (THAUS) alongside personnel with advanced technical backgrounds and aligned research objectives headed by Dr. Doug Horner and Dr. Noel Du Toit. The REMUS AUV is pictured in Figure 16 along with Aquanauts stationed at the Aquarius habitat (seen in background).

Figure 16.   Aquanauts with the NPS REMUS AUV at the Aquarius Habitat,
from [20]

A research emphasis was placed on expanding unmanned system autonomy. Autonomy enables the vehicle, through exteroceptive sensing, to make intelligent navigational decisions such as obstacle avoidance and navigation in cluttered, dynamic environments.   Underwater operations are of particular interest to NASA and CAVR research since these operations *require* unmanned system autonomy. The underwater domain not only necessitates the use of alternate means of positioning and navigation, as it is void of a ubiquitous positioning signal such as GPS, but also necessitates an alternate means of sensing and communication. Overall, the underwater domain presents a particularly unique and challenging environment for the operation of unmanned systems and as such,

The missions conducted during SEATEST II combined autonomous mapping and navigation, multi-vehicle (heterogeneous) collaboration and information sharing, joint robot-diver operations, and persistent robotic operations. The role of the NPS REMUS vehicles was to survey a nearby area with a BlueView MBE 2250 micro-bathymetry sensor. From the surveyed sonar data, an accurate bathymetry map could be built. The

bathymetry map could then be used to identify an area of interest for subsampling by the REMUS or an aquanaut, or as a navigation aid to another AUV, such as CAVR's SeaBotix vehicle.

B. EXPERIMENTAL RESULTS WITH REMUS AUV

1. Bathymetry Map Building

Over the course of a particular REMUS mission collected during SEATEST II, a total of 3,046 sonar images were captured along with the estimated vehicle state at each instance. Of the 3,046 sonar images, 2,767 of them were within range of the seafloor and thus contained usable bathymetry information. From those 2,767 images, a total of 56,491 data points were captured. The total distance traveled during the mission was approximately 6,250 meters. Figure 17 provides a perspective on the location of the SEATEST II mission relative to the Aquarius underwater habitat in Islamorada, FL. The figure was composed using the data collected during the mission and importing into Google Earth as a KML file. Each yellow dot represents the position of the REMUS vehicle when a measurement is taken.

Figure 17.   Bathymetry data points overlaid in Google Earth, from [21]

A GoPro camera was mounted underneath the REMUS vehicle just behind the BlueView micro-bathymetry sonar. Figure 18 is a snapshot from the video collected during the mission. The black cylindrical object at the top of the image is the forward-looking sonar / micro-bathymetry sonar attachment on the REMUS vehicle.

Figure 18.   GoPro image from SEATEST II mission

Overall, the terrain was composed of rock and corral formations with intermittent sandy bottomed regions. The rock and corral provided noticeable variability in seafloor depth. Depth changes were not only apparent in each individual sonar image, but also for the dataset as a whole. All 56,491 data points collected within the survey area are expressed in the LTP as a 3-D point cloud in Figure 19.
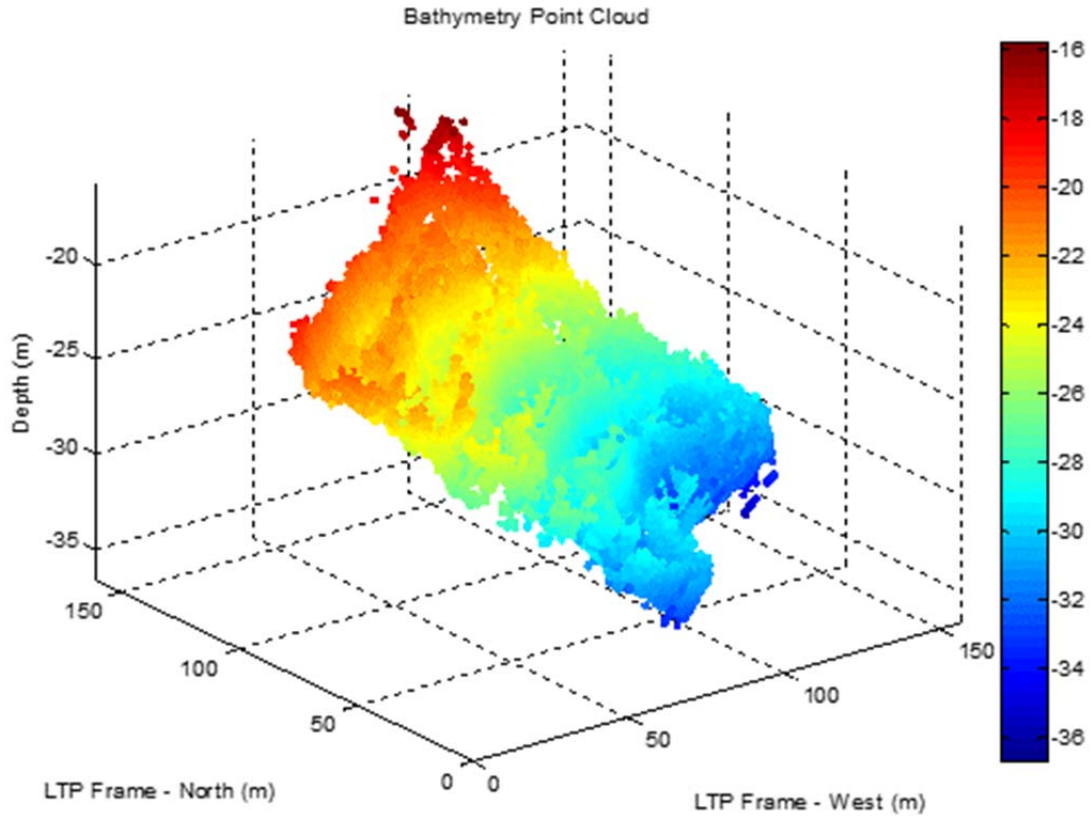
Figure 19.   3-D bathymetry point cloud

Figure 20 is also included in order to provide a different perspective of the data points collected. In Figure 20, the REMUS's entrance and exit points from the survey area can be seen, but more importantly so can the density of the points collected. In particular, associated with each turning point is a gap of no coverage. It is important to note the density of the data points throughout the surveyed area since the linear interpolation better approximates the regions that have more data points. In regions where data is sparse, the linear approximation will likely be a poor representation of the underlying topography. Passes by the AUV over the areas interpolated by data points distant from one another can expect a poorer correlation between the sonar information being seen and what the interpolated prior map shows. This will negatively impact the overall performance of the TAN solution.

For additional perspective on the dataset, the distance between each ping line is approximately two meters and the approximate size of the main survey area is 20,000

square meters. The distance between pings is due to the bathymetry sonar functioning at approximately ~ 0.5 Hz throughout the mission and the REMUS having a mission defined speed of 2 knots.
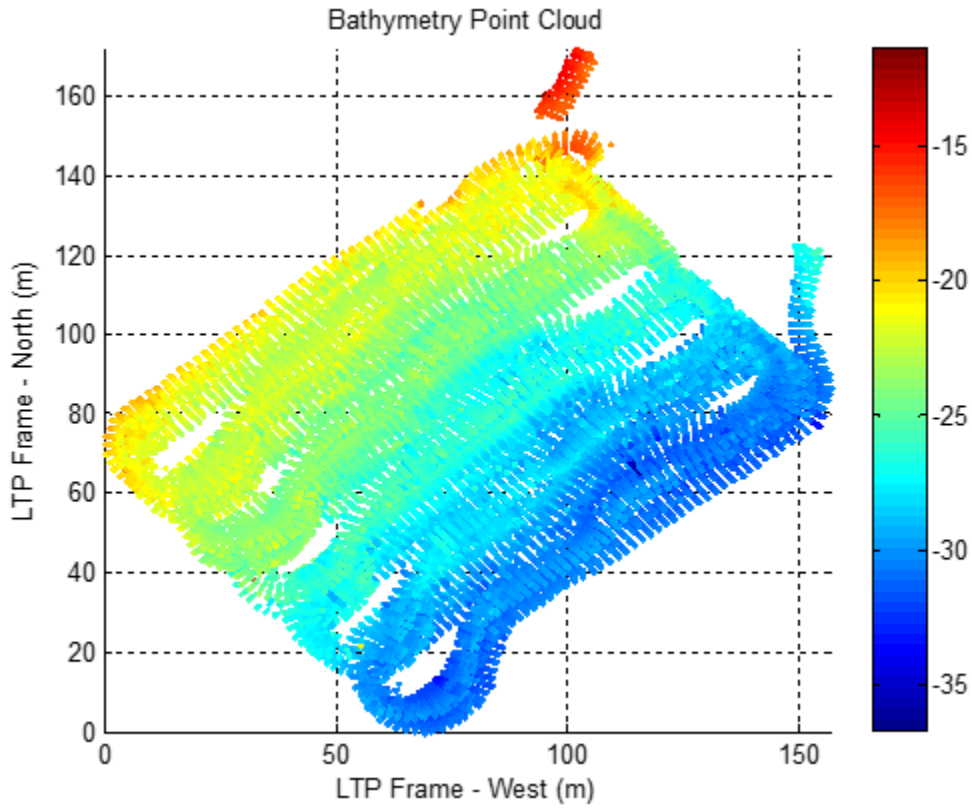

Figure 20.   An overhead perspective of the bathymetry point cloud

In order to provide complete coverage of the area surveyed, the bathymetry points were linearly interpolated to produce the results seen in Figure 21.
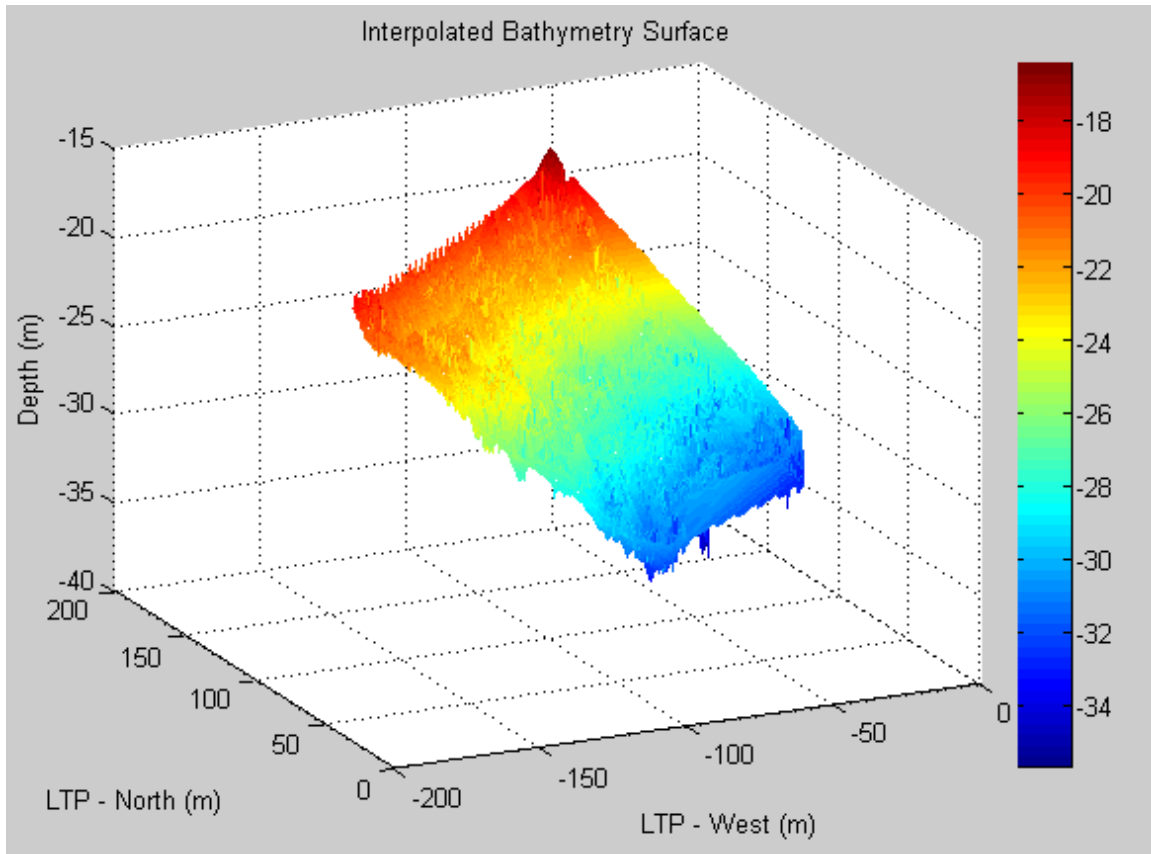
Figure 21.   Interpolated bathymetry surface

2.   Terrain Aided Navigation

Once the prior map of the surveyed area was constructed, it could be used as a navigational aid. Using the process and measurement models as a part of the particle filter, along with the output probability density function from the correlation step, an estimate of the vehicle state using the prior bathymetry map was calculated. Specifically, after the REMUS vehicle's first pass in its survey area it has already accumulated a significant amount of positional uncertainty with regard to the INS positional estimate. An example of the magnitude of the uncertainty difference between the vehicles first and second passes through the survey area is depicted in Figure 22. The amount of uncertainty accumulated through the first pass of the region was approximately 0.670 meters CEPR. By the time the vehicle passed through the area again, the positional uncertainty was approximately 8.068 meters CEPR.
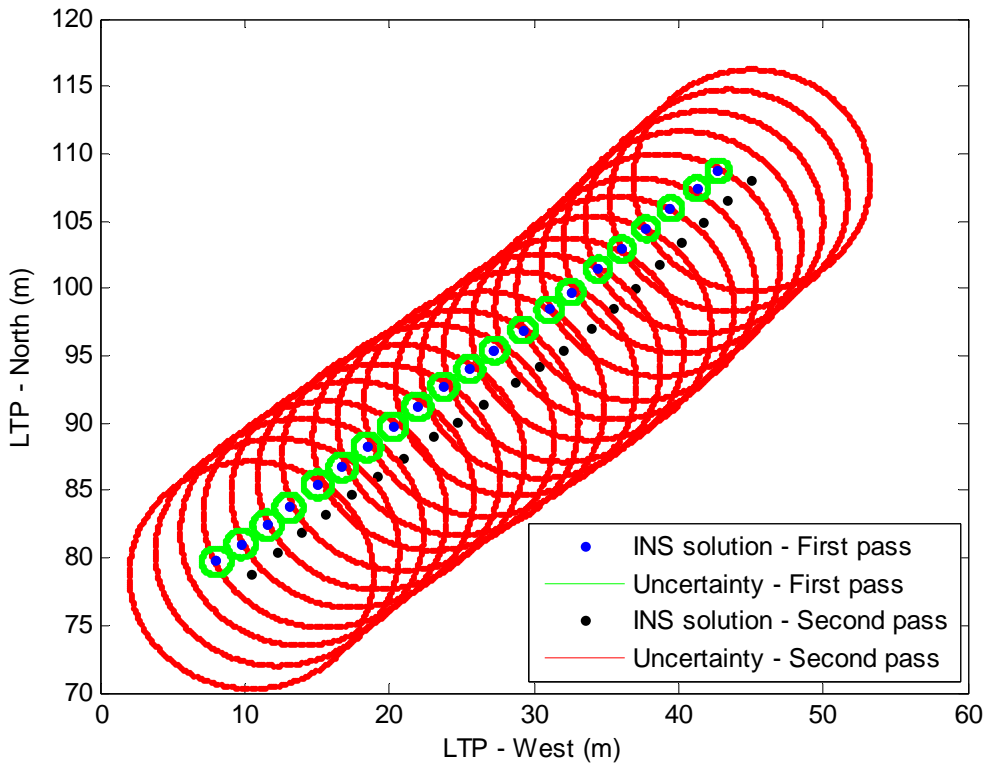
Figure 22.   Difference in uncertainty of INS positional estimation between
subsequent passes of the same region

Figure 23 is an example of the two-dimensional array represented as an intensity
image using MATLAB's colormap. Figure 24 includes red plus sign overlays on the
image that represent the altitude measurements used for each sonar ping (after
thresholding).
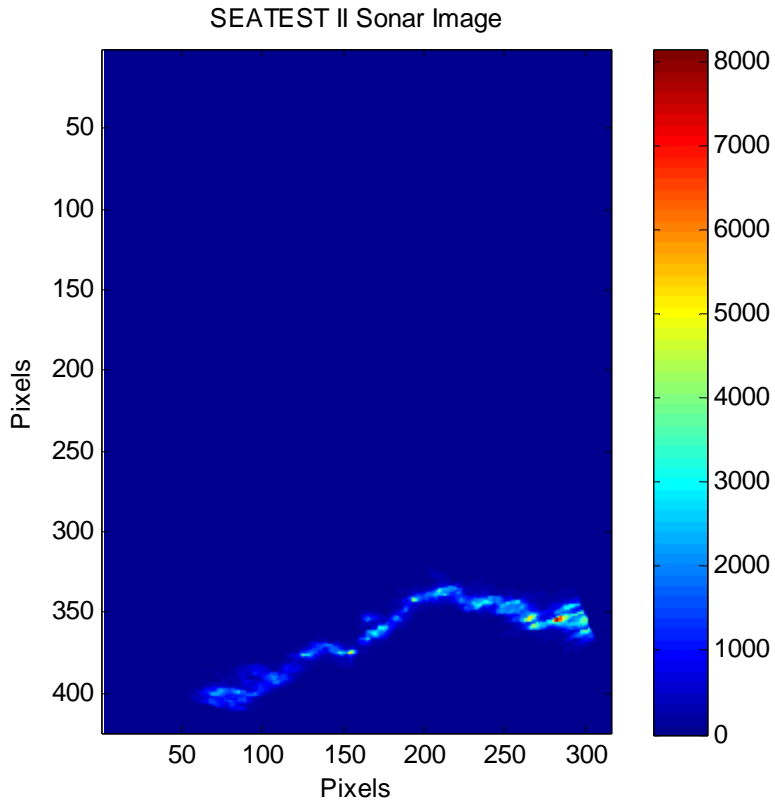
Figure 23.   Sonar image collected during SEATEST II
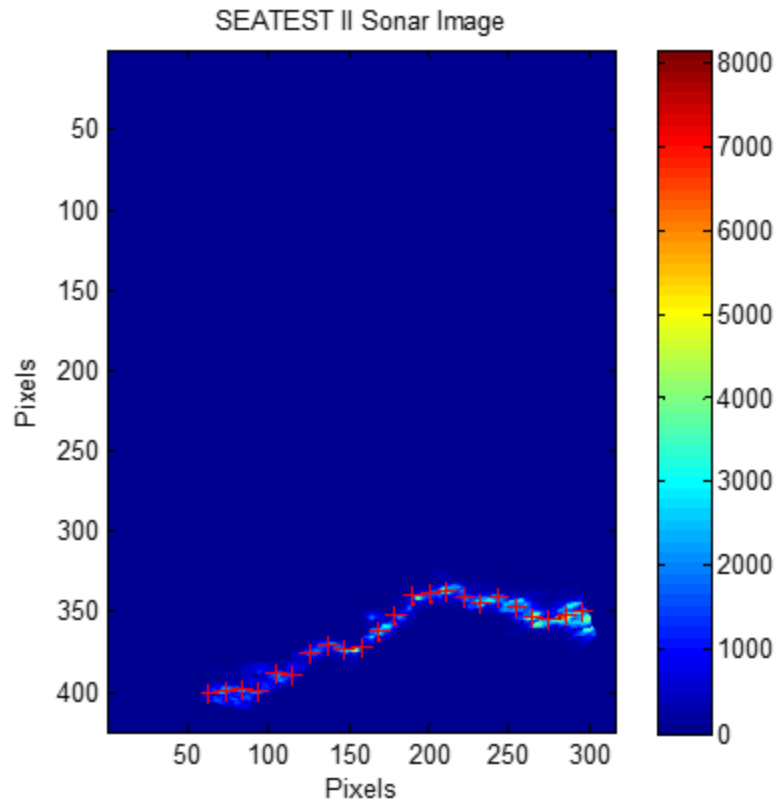
Figure 24.   SEATEST II sonar image after thresholding data points

In Figure 24, it can be seen that 23 data points were extracted. The represents a swath width of approximately 5.75 meters orthogonal to the longitudinal direction of the AUV. All 23 points then went through a coordinate transformation based upon the Euler angles and depth of the vehicle in order to be expressed in the same global frame as the prior bathymetry map. Figure 25 shows an example correlation between the 23 data points expressed in the global frame and the region of the prior map encompassing the vehicles current level of uncertainty.
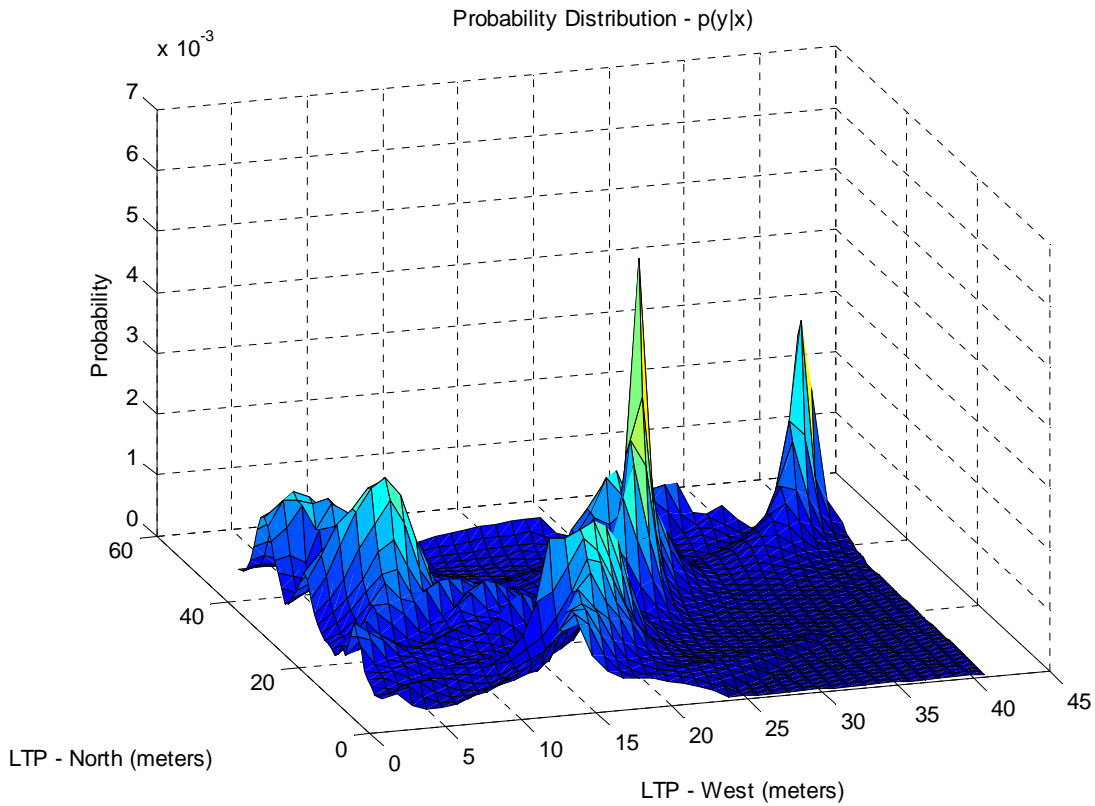
Figure 25.   Correlation probability distribution for a new sonar ping— $p\left(\boldsymbol{y}_k \mid \boldsymbol{x}_k\right)$

Figure 26 shows a sequence of four correlation plots. This provides a snapshot of the multi-modality that typically is associated with sequential pings throughout the dataset. Each plot represents a probability distribution $p\left(\boldsymbol{y}_k \mid \boldsymbol{x}_k\right)$ that is output from the correlation step and used in the recursive Bayesian filter.
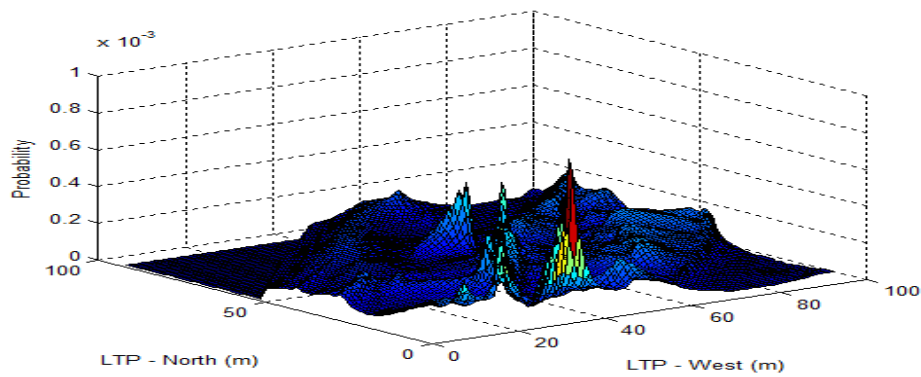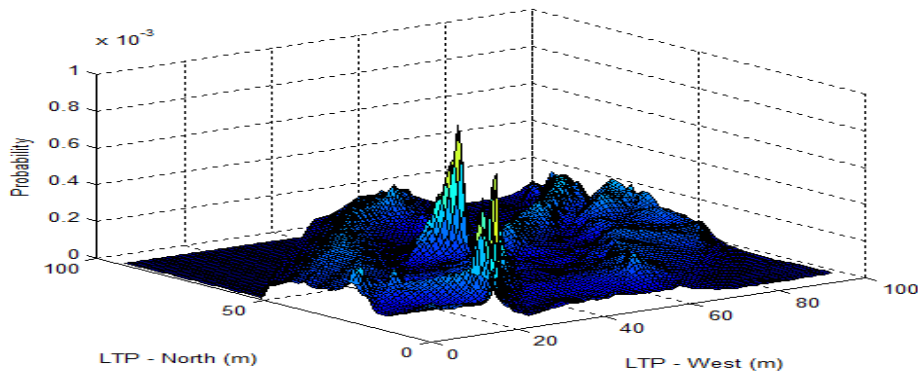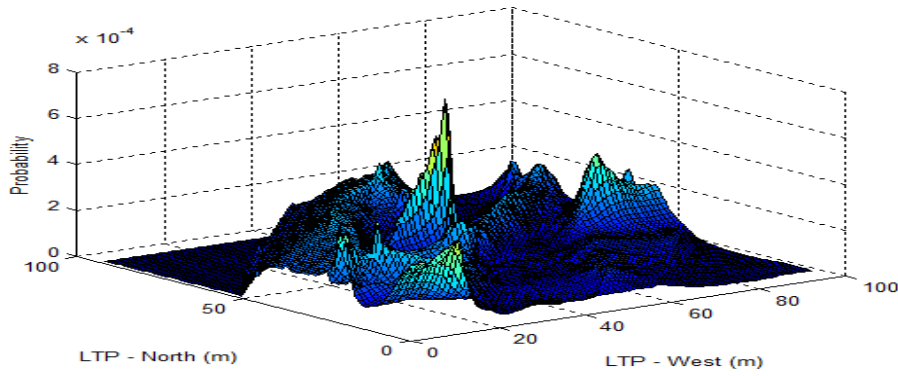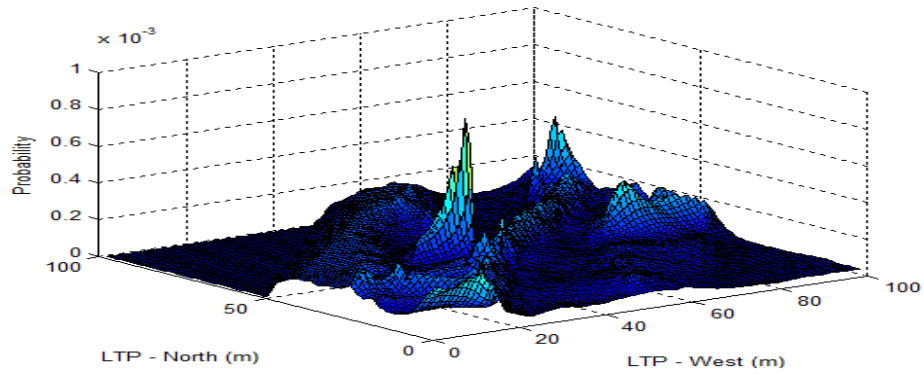
Figure 26.   Correlation probability distributions for four different sonar images

47

The processing of each sonar image, transformation of the data to the LTP reference frame, and the computation of a probability distribution based on the correlation for the ping are all done in order to provide the measurement update for the particle filter. The measurement update and the process model for the propagation of the particles are the two main components of the particle filter. The results of several particle filtering simulations are shown below.

The particle filter was first tested using 100 particles over the course of 54 micro-bathymetry sonar pings. Figure 27 is the result of this preliminary test of the particle filter algorithm.
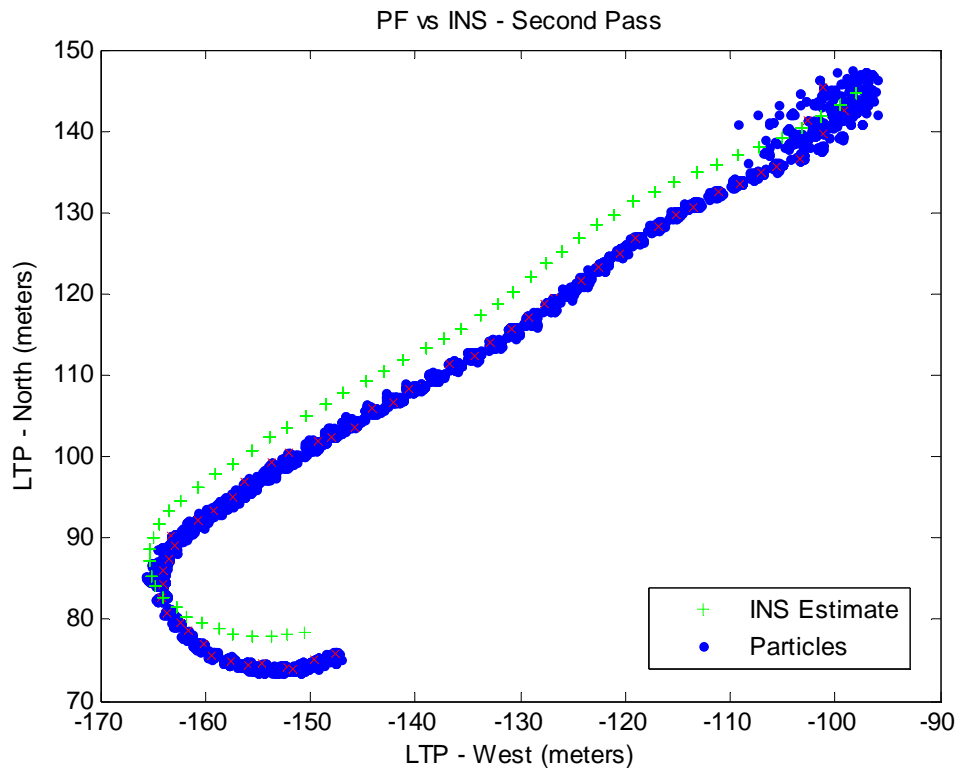

Figure 27.   Particle filter results on first leg of second pass of the survey area

Figure 27 is indicative of the rapid convergence of the particles from an initial distribution with a larger standard deviation, to a much more tightly grouped set of particles. The initial standard deviation of the particles is 3.994 meters, while eight pings

later the standard deviation is approximately 0.5 meters. While the particles at any state other than the initial state do not approximate Gaussian distributions, the standard deviation is still used here in order to provide a metric as to the spread of the particles.

With the support of preliminary results, subsequent particle filter testing was completed using 1,000 particles. Figure 28 shows the results using 1,000 particles over an entire "navigate rows" mission objective through the survey area.
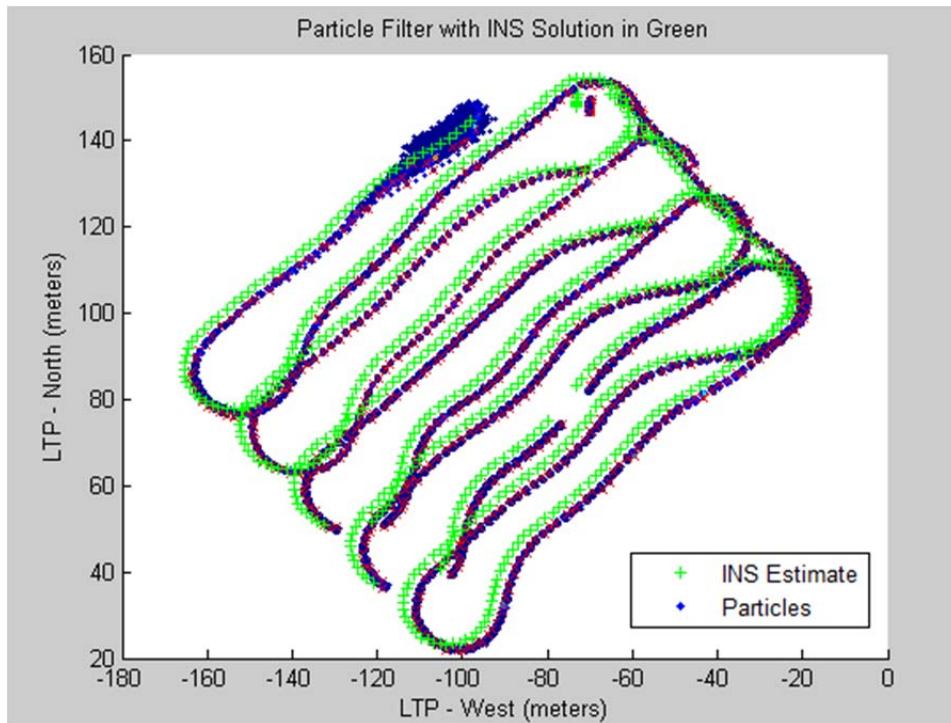
Figure 28.   Particle filter with 1,000 particles compared to INS estimation

Again, the filter can be seen to relatively quickly constrain the positional uncertainty of the AUV based upon the measurement and process updates. A GPS fix was taken at the end of the run and compared to the INS and particle filter estimations. The total positional uncertainty at the end of the run was 15.627 meters. The GPS fix was acquired using seven satellites with a horizontal error of approximately two meters. The INS solution as compared to the GPS fix was 14.272 meters away. The particle filter estimation as compared to the GPS fix was 8.863 meters away.

49

There are several error sources that can be attributed in varying degrees to the eventual particle filter estimation error of over 8 meters. GPS error, both from the initialization of the vehicle at the start of the mission and from the concluding GPS fix, could certainly account for a significant portion of the error. Additional error sources include the unaccounted for positional uncertainty in creating the prior bathymetry map, the linear interpolation of the prior map, and the particle filtering method. Within particle filtering, there can be a couple sources of error ranging from the selection of too few particles to properly approximate the probability density to the impact of various particle resampling techniques. Further literature research unveiled a detrimental effect of implementing a SIR particle filter on a vehicle with a high precision INS called "sample impoverishment" [2], [22], and [23]. A process model with small process noise, like that of the REMUS INS system, can be susceptible to a convergence on a false estimate. The particles are then propagated with small process noise and thus remain tightly clustered around a false estimate with little chance of recovery. This issue can be the result of a terrain change or artifacts in the prior map generation [22], or from premature convergence on a false estimate [23].

In order to address the concerns of sample impoverishment due to the small process noise associated with the REMUS INS, the particle filter was re-initialized shortly prior to surfacing for a GPS fix. Figure 29 is the result from this simulation.
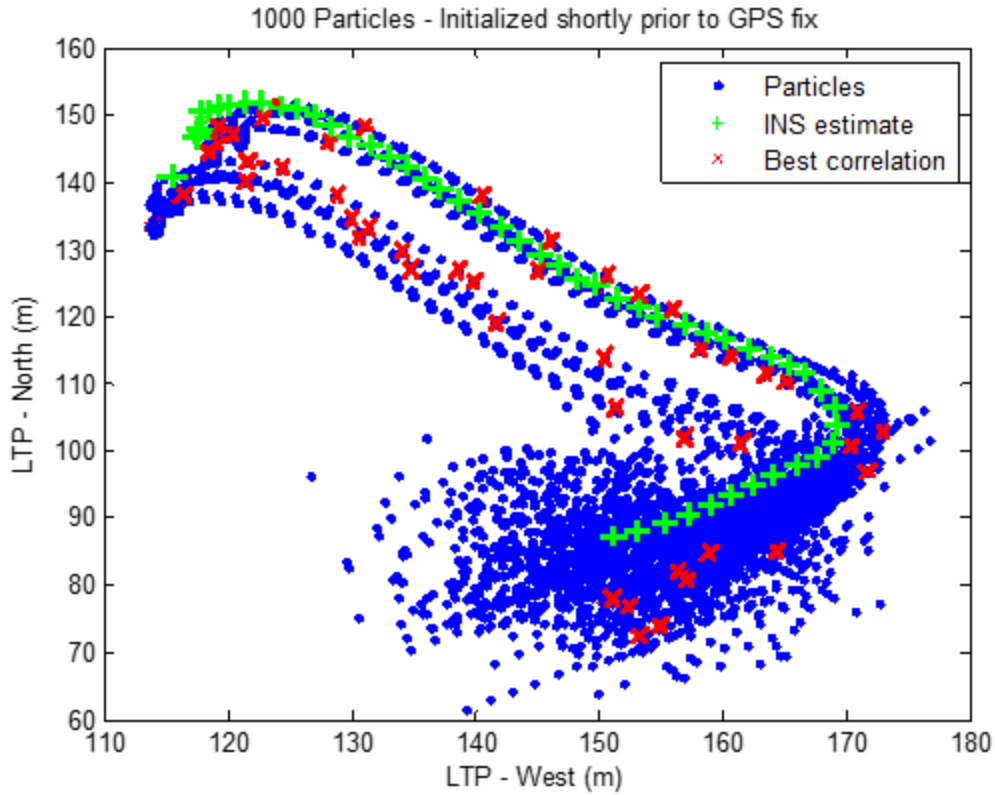
Figure 29.   Particle filter with 1,000 particles prior to GPS fix

It can be seen in Figure 29 how the particle filter did not immediately converge to a single, tightly group position estimate but instead supported multiple hypotheses as to the location of the vehicle based upon the correlations being performed. Figure 30 is provided in order to clearly visualize the GPS positional update along with the final iteration of the particle filter using 1000 particles. While there clearly are multiple hypothesis as to the position of the AUV, the red "x" indicates the position of the best correlated particle. The best correlated particle is approximately 2.846 meters away from the GPS updated navigation estimate.
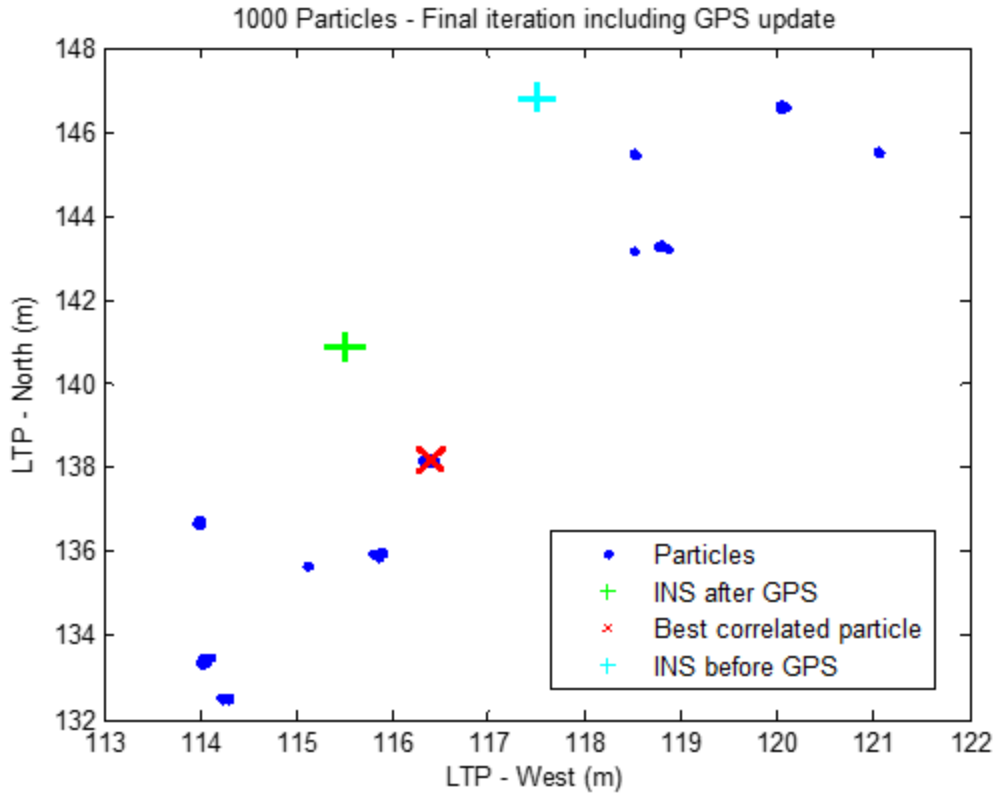
Figure 30.   Final iteration of particle filter using 1000 particles

The results from this simulation indicate that the relatively poor results from the testing of the particle filter on the full mission were substantially due to a false or premature convergence upon an estimate. Initializing the particle filter closer to the GPS fix produced significantly more accurate results. Further discussions on techniques that mitigate the chance of false convergence and sample impoverishment are discussed in the section on future work.

VI. CONCLUSIONS

A. PERFORMANCE ASSESSMENT

This thesis is the first to address terrain-aided navigation for a small, man-portable AUV. It included the entirety of the TAN process from building the prior bathymetry map as a navigational aid to the implementation and analysis of a particle filter for AUV position estimation. The combination of the ultra-high-resolution downward-looking sonar, INS and particle filter approach showed great promise for accurate underwater navigation.

That said there are many areas for improvement. They can be categorized as follows:

1. Map building
   a. Data interpolation
2. Image processing
3. Particle filter implementation
4. Real-time implementation

1. Map Building

One of the most significant challenges in building an accurate bathymetry map is accounting for the inherent, growing uncertainty associated with the INS of the AUV. The problem poses quite a conundrum. Through TAN methods, one wishes to localize the position of the vehicle through the use of a prior map due to accumulating uncertainty with regards to position. However, the prior map is built using the INS solution, with its growing uncertainty, in the first place. Therefore, additional research is recommended into building a more accurate prior bathymetry map. A relatively simplistic fix to the bulk of this issue would be to survey an area using an LBL system. Although this would not eliminate the uncertainty with regards to the vehicle and thus the map, it would constrain it. Other potential methods of building a more accurate map could be the use of a quad-tree data structure that stores data different resolution grids based upon the certainty of the estimate or through ensuring consistency of the map by feature based correction

methods. This would entail a similar correlation technique as proposed above, but this correlation would be utilized in ensuring consistency with regards to the locations of features in the map. Overall, the vehicular positional uncertainty while building a bathymetry map should be taken into account, and methods for doing so are currently being researched. The fact that this was not taken into account in building the prior bathymetry map is a primary suspect for the poorer than expected accuracy of the particle filter.

a. *Data Interpolation*

As mentioned in the data interpolation paragraph, the *TriScatteredInterp* MATLAB function was used in order to perform a simple linear interpolation through all of the data points. A potentially more sophisticated method of interpolation (e.g., Kriging, Gaussian random fields or compressive sampling) takes into consideration the two-dimensional signal and the variance of the data may lead to a more accurate underlying map.

2. Image Processing

The sonar image processing algorithm utilized on this particular dataset worked efficiently and effectively. However, the algorithm is not robust to any significant changes in the environment. Poor performance could be expected in more dynamic, cluttered environments. In particular, testing in a harbor or kelp field would necessitate a more advanced and robust image processing algorithm. As a start, an adaptive threshold for identifying returns associated with the sea floor in various different environments with different bottom compositions would be useful. Additional work may be done to mitigate the effects of any noise that may appear in a dataset (noise was not a significant issue in the dataset collected). Nonetheless, the resolution of the data extracted from the image is only constrained by the fundamental pixel to meter ratio of 0.023052 and therefore the resolution could be increased at any point if it would be deemed worth the extra computational burden. More importantly, some changes on the image processing algorithm itself may be advised.

3. Particle Filter Resampling Technique

As mentioned, the SIR particle filter implementation suffers from sample impoverishment. The sample impoverishment is largely attributed to the small process noise associated with the high-grade INS of the REMUS vehicle. A few methods that help counteract or negate this effect are discussed in [2], [22], and [23]. In particular, the Rao-Blackwellization of the particle filter as described in [2] is the recommended course of action for future work. Not only will Rao-Blackwellization help combat the effects of small process noise on the particle filter solution, but it will also reduce computational complexity and should improve accuracy [2], [5]. Other potential solutions include re-initializing the particle filter with a much large covariance when an error in estimation has been detected [22], using a genetic algorithm [23], or through the use of a different particle filter resampling technique such as the *resample-move* algorithm described in [24] or the *regularization* method described in [25].

4. Real-time Implementation on REMUS 100 AUV

Perhaps most importantly, the end goal of this line of research is to implement a real-time system on CAVR's REMUS 100 AUV. Concerns as to the long-term accuracy of the particle filtering solution should be addressed prior to fully trusting the navigation solution provided by the particle filter. Notwithstanding these concerns, the work provided thus far is suited to experimental testing on the REMUS vehicle. Real-time implementation would be the next major step in advancing TAN for an AUV.

THIS PAGE INTENTIONALLY LEFT BLANK

LIST OF REFERENCES

[1]   S. Carreno, P. Wilson, P. Ridao, and Y. Petillot, "A survey on terrain based navigation for AUVs," *Oceans*, pp. 1–7, 2010.

[2]   T. Schon, F. Gustafsson, and P.J. Nordlund, "Marginalized particle filters for mixed linear/nonlinear state-space models," in *IEEE Transactions on Signal Processing*, vol.53, no.7, pp. 2279–2289, Jul. 2005.

[3]   H. Feder, J. Leonard and C. Smith, "Adaptive sensing for terrain aided navigation," in *Oceans Conference Proceedings*, pp. 336–341, 1998.

[4]   L. Stutters, H. Liu, C. Tiltman, and D. J. Brown, "Navigation technologies for autonomous underwater vehicles," in *IEEE Transactions on Systems, Man, and Cybernetics, Part C: Applications and Reviews*, vol. 38, pp. 581–589, 2008.

[5]   F. Gustafsson, F. Gunnarsson, N. Bergman, U. Forssell, J. Jansson, R. Karlsson, and P. Nordlund, "Particle filters for positioning, navigation, and tracking," in *IEEE Transactions on Signal Processing*, vol. 50, pp. 425–437, 2002.

[6]   P. Nordlund, "Sequential Monte Carlo Filters and Integrated Navigation," M.S., Dept. of Elect. Eng., Linköpings University, Linköpings, Sweeden, 2002.

[7]   K. B. Anonsen and O. Hallingstad, "Terrain aided underwater navigation using point mass and particle filters," in *Proceedings of the IEEE/ION Position Location and Navigation Symposium*, San Diego, CA, 2006.

[8]   S. Dektor and S. M. Rock, "Improving robustness of terrain-relative navigation for AUVs in regions with flat terrain," in *IEEE AUV*, pp. 1–7, 2012.

[9]   F. Teixeira, A. Pascoal, and P. Maurya, "A novel particle filter formulation with application to terrain-aided navigation," in *IFAC Workshop on Navigation, Guidance, and Control of Underwater Vehicles*, Porto, Portugal, 2012.

[10]   *Autonomous underwater vehicle—REMUS 100*. Kongsberg, Norway: Kongsberg Maritime. [Online]. Available: http://www.km.kongsberg.com/ks/web/nokbg0240.nsf/AllWeb/D241A2C835DF4 0B0C12574AB003EA6AB?OpenDocument

[11]   *KN-9050 SEADeViL System Characteristics*. Little Falls, NJ: Kearfott Corp., 2012.

[12]   *REMUS Operations and Maintenance Manual*. Kongsberg, Norway: Kongsberg Maritime.

[13]   N. A. McChesney, "Three-dimensional feature reconstruction with dual forward looking sonars for unmanned underwater vehicle navigation," M.S. thesis, Naval Postgraduate School, Monterey, CA, 2009.

[14]   *MB2250-N / MB2250—W MicroBathymetry Sonar*. Teledyne BlueView, Bothell, WA, 2009.

[15]   Monterey Bay Aquarium Research Institute, "The AUV maps the seafloor with a swath of sound." [Online]. Available: http://www.mbari.org/auv/MappingAUV/sonars.htm

[16]   "MATLAB and statistics toolbox release 2012b," The MathWorks, Inc., Natick, MA, 2012.

[17]   G. Welch and G. Bishop, "An introduction to the Kalman filter," M.S. thesis, Univ. of North Carolina, Chapel Hill, NC, 2006.

[18]   M. S. Arulampalam, S. Maskell, N. Gordon, and T. Clapp, "A tutorial on particle filters for online nonlinear/non-Gaussian Bayesian tracking." *IEEE Transactions on Signal Processing*, vol. 50, no. 2, pp. 174–188, Feb. 2002.

[19]   J. J. Martinez-Espla, T. Martinez-Marin, and J. M. Lopez-Sanchez. "A particle filter approach for InSAR phase filtering and unwrapping," *IEEE Transactions on Geoscience and Remote Sensing*, vol. 47, no. 4, pp. 1197–1211, 2009.

[20]   D. Horner and N. du Toit, "Evaluating the Utility of Robotic Technologies for Joint Human-Robot Missions," Center for Autonomous Vehicle Research, NPS, Monterey, CA. 2013.

[21]   NOAA Aquarius Underwater Laboratory, Islamorada, FL. 24.950ºN and 80.454ºW [image]. (May 2014). Available: Google Earth.

[22]   S. M. Rock, S. G. Dektor, and S. E. Houts, "Robust Framework for failure detection and recovery for terrain-relative navigation," Aerospace Robotics Laboratory, Stanford Univ., Palo Alto, CA, 2012.

[23]   P. Seongkeun, H. Jae Pil, K. Euntai, and K. Hyung-Jin, "A New Evolutionary Particle Filter for the Prevention of Sample Impoverishment," in *IEEE Transactions on Evolutionary Computation*, vol. 13, no. 4, pp. 801–809, Aug. 2009.

[24]   W. R. Gilks and C. Berzuini, "Following a moving target—Monte Carlo inference for dynamic Bayesian models," *J. R. Statist. Soc. B*, vol. 63, pp. 127–146, 2001.

[25]   C. Musso, N. Oudjane, and F. LeGland, "Improving regularized particle filters," in *Sequential Monte Carlo Methods in Practice*, A. Doucet, J. F. G. de Freitas, N. F. Gordon, Eds. New York: Springer-Verlag, 2001.

INITIAL DISTRIBUTION LIST

1.   Defense Technical Information Center
        Ft. Belvoir, Virginia

2.   Dudley Knox Library
        Naval Postgraduate School
        Monterey, California